Determination of Interfacial Bond Behavior of Composite Concrete-Asphalt Pavement Systems

FHWA-RIDOT-RTD-08-1
June, 2008

Dr. Martin Sadd
Dr. Arun Shukla
Venkat K.S. Subramaniam, MS
Department of Mechanical Engineering and Applied Mechanics

and

Dr. K. Wayne Lee
Department of Civil & Environmental Engineering

University of Rhode Island
Kingston, RI 02881

Sponsored By

Rhode Island
Department of Transportation

RESEARCH AND TECHNOLOGY

Technical Report Documentation Page

1. Report No.	2. Government Accession No.	3. Recipient's Catalog No.
RIDOT-RTD-08-1	N/A	N/A

4. Title and Subtitle	5. Report Date
Determination of Interfacial Bond Behavior of Composite Concrete-Asphalt Pavement Systems	June, 2008
	6. Performing Organization Code: N/A

7. Author(s)	8. Performing Organization Report No.
Dr. Martin Sadd, Dr. Arun Shukla, Dr. K. Wayne Lee, Mr. Venkat K.S. Subramaniam	

9. Performing Organization Name and Address	10. Work Unit No. (TRAIS)
College of Engineering University of Rhode Island Kingston, RI 02881	N/A
	11. Contract or Grant No.: N/A

12. Sponsoring Agency Name and Address	13. Type of Report and Period Covered
Rhode Island Department of Transportation Two Capitol Hill, RM 013 Providence, RI 02903-1124	Final
	14. Sponsoring Agency Code: SPR-2(29)-2284 A study conducted in cooperation with RIDOT

15. Supplementary Notes

16. Abstract

Described herein is a study of the interfacial debonding behavior between concrete and asphalt pavement material as found in whitetopping pavement applications. The study includes the interfacial failure resulting from both static and dynamic loading. Studies under static conditions used interfacial fracture mechanics techniques to investigate and characterize the behavior of pre-existing cracks along the asphalt-concrete interface. Experimental laboratory testing was done on uniaxially loaded rectangular block samples using asphalt material from two different age groups. It was found that the fracture toughness and interface strength increased with aging. Experiments were conducted with interfaces both normal and inclined to the loading direction, thereby allowing variation in the shear loading component. Results indicated that as shear loading component increased, the interface strength also increased. Finite element analysis was also used to explore the stresses in the laboratory block sample geometry. Finite element results of the stress distribution near the interfacial crack compared reasonably well with predictions from an idealized analytical solution. A special lap-joint specimen geometry was developed to determine the dynamic interfacial shear strength of bonded specimens using a Split Hopkinson Pressure Bar (SHPB) loading apparatus. Because of the small sample size, no pre-existing interface crack was used in this testing. Lap-joint samples were tested under both static and dynamic loading. Results indicated that at high loading rates the shear strength of the bonded lap joint was found to be about four times its static value.

17. Key Word	18. Distribution Statement
whitetopping, concrete, asphalt, interface debonding, interfacial fracture	No restrictions. This document is available to the public through the Nation Technical Information Service, Springfield, Virginia 22161

19. Security Classif. (of this report)	20. Security Classif. (of this page)	21. No. of Pages	22. Price
Unclassified	Unclassified	66	N/A

Form DOT F 1700.7 (8-72) Reproduction of completed page authorized

DISCLAIMER

A University of Rhode Island (URl) research team prepared this report for the Rhode Island Department of Transportation (RIDOT). The contents of the report reflect the views of the URl research team, which is responsible for the accuracy of the facts and data presented herein. The contents are not to be construed as the official position of the RIDOT or URI. This document does not constitute a standard, specification or regulation.

Citation of trade or manufacturer's names does not constitute an official endorsement or approval of the use of such commercial products. Trade or manufacturer's names appear herein solely because they are considered essential to the object of this study.

ACKNOWLEDGEMENTS

We would like to thank the Rhode Island Department of Transportation for the financial support given to make this study possible. In particular we thank Colin Franco and Francis Manning of the Research and Technology Section for their support, guidance and discussions. We also thank RIDOT staff members Michael Sock and Jan Bak who helped supply some core samples and related equipment. Acknowledgement is also given to P.J. Keating and Grace Corporations for their generous supply of raw materials needed for laboratory sample preparation. We also express thanks to several URI shop and staff members including Kevin Donovan, Kevin Brocollo and Matt Freeman for their help in various machining operations necessary for laboratory testing program.

TABLE OF CONTENTS

LIST OF TABLES

LIST OF FIGURES

CHAPTER I – INTRODUCTION

1.1 Background

Most of the national highway systems, constructed during the 1960s, have passed the end of their original design life. The rehabilitation of this enormous aging system poses a significant economic and technical problem to federal, state and town agencies across the nation. As presented by Cho and Koo (2003), over the past few decades, many states have explored the use of a *whitetopping rehabilitation technique*, whereby a relatively thin layer of concrete is applied over a distressed segment of asphalt. For example, during the 1970's California used concrete overlays on several sections of existing asphalt highways. Minnesota used a similar method for flexible low volume road pavements in 1990, and the technique has also been used in Iowa for many years. Concrete overlays have also been used for bridge deck pavement rehabilitation. Most recently, the Rhode Island Department of Transportation installed a whitetopping section in the town of Lincoln. A schematic of the w*hitetoppin*g technique is shown in Fig. 1.1. The method consists of using a Portland Cement Concrete (PCC) overlay on top a hot mix asphalt (HMA) roadway. Typically the surface of the asphalt is milled or reworked to create a relatively smooth and clean surface before the concrete is applied.

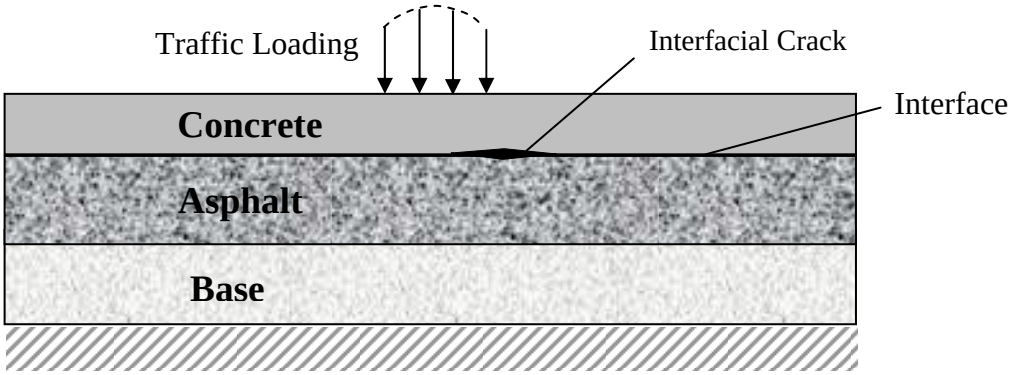

Fig. 1.1 Concrete Overlay on Top of Typical Asphalt Pavement

Traditional concrete pavements are designed to absorb energy by bending, and thus are made thick enough to resist stresses induced by bending. Conventional concrete overlays have been used in heavy truck corridors to combat asphalt rutting. These concrete overlays generally have a minimum thickness of 5in (127mm) and are commonly designed with the assumption that little to no bonding occurs between the existing pavement and the concrete overlay. In some

cases, plain and fiber reinforced concrete have been used to overlay the asphalt pavements. Concrete overlays on pavements generally offer the following improvements:

- strengthen the pavement structure against further deterioration due to fatigue cracking, rutting, and other effects
- improve smoothness and restore ride quality
- add skid resistance.

Properly constructed concrete overlays are durable and can considerably extend the service lives of existing facilities. Based on the thickness of the PCC overlay, such methods are commonly designated as thin whitetopping (TW) or ultra-thin whitetopping (UTW). Thin whitetopping (TWT) refers to a 4 to 6in (102 to 152mm) overlay while ultra-thin-whitetopping (UTW) typically includes PCC layers of about 2 to 4in (50 to 102mm). The first 2in (50mm) UTW experiment, conducted in Kentucky in 1991 showed that the corner cracking was the most predominant pavement distress and joint spacing had a significant effect on the rate of corner cracking. Joint spacing of 2ft (0.6m) showed considerably less cracking than 6ft (1.8m) joint spacing. The short joint spacing is expected to reduce the moment arm of the applied load, and thus minimizes the stress due to bending. American Concrete Pavement Association (ACPA) recommends that maximum joint spacing for UTW is 12-15 times the slap thickness.

The concrete overlay reduces the tensile stresses in the pavement through increasing the thickness of the pavement and the stiffness, thereby increasing its fatigue life. A key factor influencing the overlay performance is the bond between the concrete and asphalt, and significant steps are usually taken to ensure sufficient bond is achieved. This can be done by various surface preparations of the existing pavement to produce a clean and roughened surface that will promote bonding of the freshly laid concrete overlay.

A commonly used surface preparation technique is milling the asphalt pavement. Milling is most effective for repair of rutting and shoving problems in the existing asphalt, and this practice can be used if there is adequate serviceable asphalt thickness remaining in the pavement. Heavily distressed pavement areas such as large cracks and potholes are normally repaired prior to the placement of any whitetopping layer. In general milling smoothes out surface distortions establishes appropriate cross-slopes and grade lines and provides a proper surface for good concrete bonding. Typically, after all surface preparation activities have been completed, the existing asphalt surface is cleaned to remove any dust, dirt, or other particles or debris that may

be detrimental to the desired bonding. Sometimes water fogging and/or whitewashing the existing asphalt is also used just prior to concrete placement. Whitewashing commonly uses a lime slurry spray (water and hydrated lime) to cool and enhance the asphalt surface for concrete overlay.

1.2 Literature Review

Distress surveying and failure identification of UTW pavement were recently reported by Nelson et al. (2002) and Vandenbossche et al. (2002). They observed mainly distress types including: debonding and interface cracking, corner cracking, and mid-slab transverse and longitudinal cracking. The amount of cracking that occurred in sections under study was found to be a function of the joint layout. Reducing the panel size will reduce the curling/warping and the traffic load related flexural stress. Many of the observed transverse cracks are a result of previously existing temperature cracks in the asphalt reflecting up through the concrete. Vehicle loading will increase the normal and shear stresses at the interface, thereby encouraging crack propagation up from the interface. Nelson et al. (2002) indicated that corner cracking behaviors are caused when the interfacial stresses exceed the material strength, and several different scenarios were described where this could occur. Mid-slab transverse and longitudinal cracks have also been reported and are initiated by tensile stresses from traffic wheel loading. Other issues related to delamination behavior lie in the mismatch in elastic and inelastic material properties of the layers. In Tennessee several experiment constructions were made to do research on deterioration of a UTW layer and it was reported that the thickness and conditions of the asphalt layer had influenced the deterioration. As mentioned significant maintenance and repair cost can be achieved with an appropriate use of UTW and in particular we can say that the thickness of the asphalt pavement influences the performance. Colorado DOT and ACPA have established design specifications for whitetopping.

The bond strength between HMA pavement and PCC is directly related to the interface properties. Interface fracture mechanics can be employed to study the behavior of interfacial cracks. Previous work conducted by Hutchinson et al. (1987) and Rice (1988) determined linear elastic solutions for interfacial cracks and developed solutions to calculate the stress intensity factors for both mode I (opening deformation) and mode II (shear deformation) problems. The stress intensity factor is an important concept in fracture mechanics studies and it generally can

be used to determine the material's resistance to fracture (i.e., fracture toughness). In essence, the tensile and shear effects near the crack tip are intrinsically linked and therefore inseparable. In later work, Rice, Suo and Wang (1990) presented elastic-brittle fracture theory for interface cracks, in which two dimensional singular interfacial crack tips stress fields are given. Additional interface work by Ricci et al. (1997) utilized strain fields to experimentally characterize the behavior of interfacial cracks under quasi-static load conditions. McBride et al. (2002) investigated concrete and aluminum silicate bimaterials and characterized the behavior of interfacial cracks under quasi-static load conditions and discussed the postmortem analysis.

Additional bimaterial interface studies have used lap joint specimens, analyzing stresses under static loading using elasto-plastic finite element methods, two dimensional elasticity theory and mathematical modeling of adhesive lamina. Chen and Cheng et al. (1983) analyzed adhesive-bonded single lap joints using two dimensional elasticity theory in conjunction with the variational principle of complimentary energy. Previously, Rossmanith and Shukla et al. (1981) and Zachary and Burger et al. (1980) investigated the stresses in a short single lap joint under dynamic loading under photoelasticity. Shukla and Srivastava et al. (2000) determined the dynamic shear strength for a lap joint specimen using classical Split Hopkinson pressure bar (SHPB) technique in compression. The joint shear strength was determined from the maximum transmitted load, assuming it was transferred predominantly as shear through the bonded joint.

Several finite element studies have been conducted to study interfacial behavior between HMA pavement and PCC layer. Nelson and Rasmussen (2002) utilized a two-dimensional finite element model, NSLIP2000, to predict the shear and normal stresses at the interface. Linear four-node slip finite elements were used to simulate interfacial behavior. Cho et al. (2003) and Kumara et al. (2003) developed three-dimensional finite element model (using ABAQUS) to investigate the problem. Additional numerical studies of the interface problem have been conducted by Nishiyama et al. (2003) who investigated the mechanical behavior of UTW pavement under stationary and moving traffic loading, allowing for viscoelastic asphalt properties. Nishiyama et al. investigated the correlation of the critical stresses with different bond levels. These simulation models showed that the thickness and elastic moduli of the asphalt and concrete layers, and layer bond strength have significant effects on the problem behavior.

1.3 Purpose of the Study

Pavement and bridge rehabilitation efforts using overlays of concrete on asphalt create a composite structure that can provide significant performance improvements. However, the resulting layered composite can also lead to premature failure commonly resulting from interfacial debonding between the concrete and asphalt. Combining the higher modulus PCC material with the softer HMA product through a bonding process produces a composite system with complex load carrying and failure behaviors. Such behaviors would depend on geometric parameters such as segment thickness and joint spacing, bonding characteristics and moduli and constitutive properties of the different materials. With many observed longitudinal and transverse cracking patterns found in TW and UTW projects, it would appear that fracture mechanics theory could help provide a better understanding of such failures. Also supporting this premise, is the expectation that construction methods along with environmental conditions will create a composite roadway with numerous interfacial cracks (see Fig. 1.1). Furthermore, traffic loadings can produce tensile, compressive and shearing stresses along the composite pavement interface, and thus the effects of each of these specific loadings need additional study. Finally, all previous studies of this composite roadway system have been made under static loading conditions. Since it is well known that these materials exhibit rate dependent deformation behaviors, it was felt that some testing under dynamic loading should be made.

Based on these observations, the study has focused attention on the following experimental, theoretical and computational components:

1. Conduct laboratory testing of composite concrete/asphalt block samples with pre-existing interfacial cracks loaded under tension to determine fracture toughness and study the detailed nature of interface debonding failure. Explore sample loadings that generate both tensile and shearing interfacial stresses. Also, conduct similar testing on samples sectioned from in situ core materials from the existing RIDOT whitetopping project.
2. Using fracture mechanics theories, determine critical stress intensity factors for both opening and shearing deformation modes of bimaterial samples.
3. Combine studies from items 1 and 2 to determine critical stress intensity factors (fracture toughness) for concrete/asphalt block samples, and compare with corresponding values of concrete and asphalt alone.

4. Conduct preliminary finite element analysis on composite block samples to verify theoretical estimates of stress fields near the interfacial cracks.
5. Conduct rate dependent studies on lap joint samples in order to compare static versus dynamic failure behaviors.
6. Explore other composite specimen geometries that may lead to easier sample preparation and yield better test results.

The primary goal of these efforts is to provide a better fundamental understanding of the interfacial failure behaviors between such concrete/asphalt composite roadways and thereby provide information that could lead to improved methods to construct such roadways.

CHAPTER II – PREPARATION OF SAMPLES

2.1 Introduction

This chapter outlines sample preparation procedures for the laboratory testing program that involved both composite block and lap joint specimens as shown in Fig. 2.1. The samples required for such testing must be a composite composed of both concrete (PCC) and asphalt (HMA) with geometry of sufficiently simple shape to allow standard testing in an Instron testing machine. It should be noted that neither sample corresponds to a ASTM standard. The interface between the two materials was kept as planar to allow for simple sample preparation, failure observation and theoretical/numerical calculations. For each sample type, the asphalt portion was prepared first and was then joined to the concrete through specially prepared molds. The sample preparation process required several steps that will now be discussed in detail.

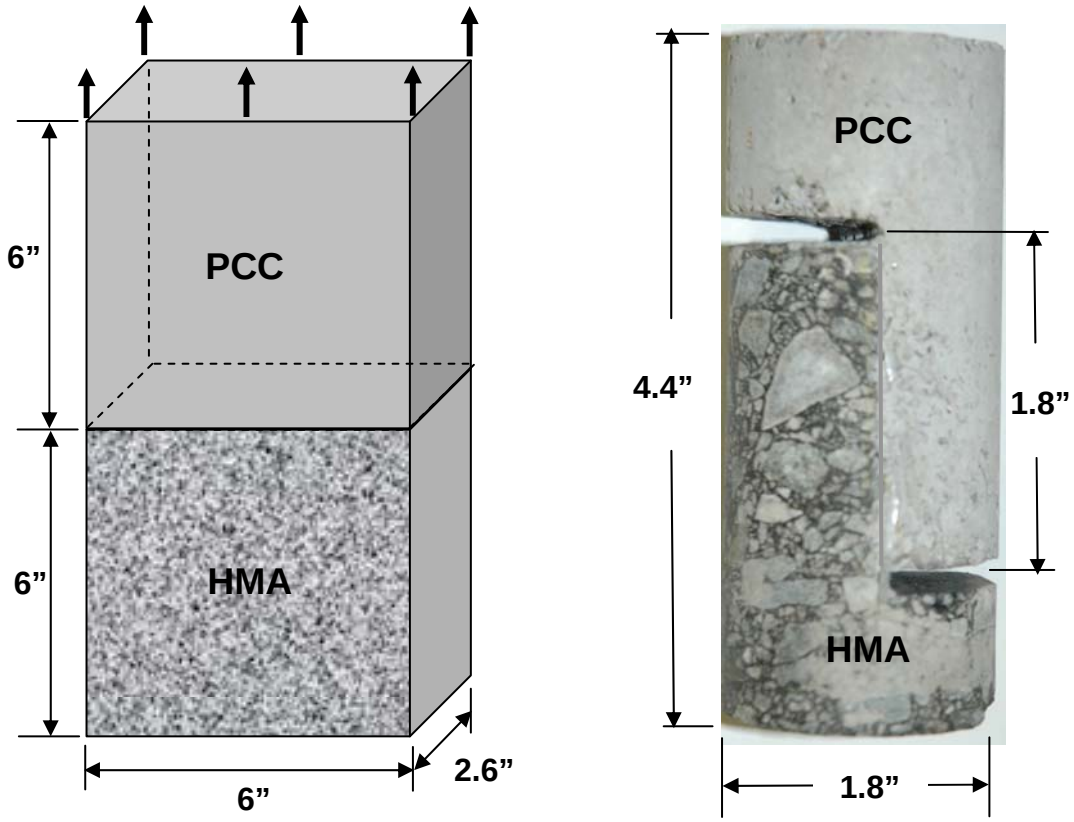

(Block Sample) (Lap Joint Sample)

Fig. 2.1 Laboratory Sample Geometries

2.2 Preparation of Asphalt Material for Block Samples

Since the block sample geometry required rectangular specimens with dimensions shown in Fig. 2.1, the asphalt portion was prepared using non-ASTM standard procedures. An Instron testing machine was used to provide compression to the asphalt block to achieve appropriate consolidation of the sample. This consolidation scheme was compared with standard Marshall specimen procedures and the specimen was found to be in the proper range specified by RIDOT. As recommended by RIDOT, PG 64–22 asphalt binders were used and the Optimum-Asphalt Content (OAC) was 5.8% of the total weight. The binder was purchased from Hudson, Inc in Rhode Island.

The raw materials of sand and aggregates were obtained from P.J.Keating, Inc of Rhode Island. At the facility, the bin size corresponds to the manner in which the raw materials are stacked at the plant. The nominal maximum size is one size larger than the first sieve to retain more than 10 % of the material. There are basically two types of raw materials involved, namely, stone and sand. The collected materials were dried in an oven, sampled and used for sieve analysis to obtain the percentage of aggregates according to the standard size ranges. The Job-Mix Formula (JMF) was obtained from RIDOT and is given in the Table 2.1. The gradation chart for this mix is shown in Fig 2.2.

Table 2.1 Aggregate Gradation

Aggregate Size	**% Passing**
-3/4 + ½	7
-½ + 3/8	11
-3/8 + #4	22
-#4 + #8	16
-#8 + #30	20
-#30 + #50	7
-#50 + #100	7
-#100 +#200	5
-#200	5

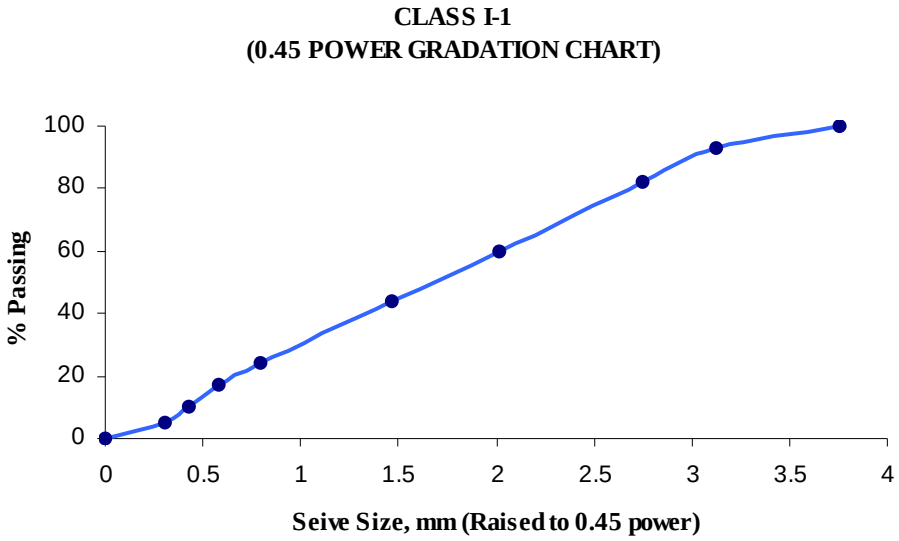

Fig. 2.2 Gradation Chart

2.3 Asphalt Block Sample Preparation

Because of requirements in fracture mechanics-testing, the prepared asphalt sample portion was required to be rectangular in shape. Since there is no known standard ASTM procedure to follow for such sample preparation; it was decided to follow a similar procedure as specified by Tekalur et al. (2004). The specimen was prepared by compacting hot mix aggregates and asphalt in a specially designed and constructed mold. Compaction was achieved by using an Instron testing machine. The level of compaction was found by trial and error and experimental verification of the properties was compared to the standard Marshall specimen. The final compaction loading history was comprised of a repeated load of 85kN applied in 12 cycles with the last cycle held constant for about 10min before the mold is removed. The bulk specific gravity of the rectangular block sample was determined and several trials are shown in the Table 2.2.

Table 2.2 Bulk Specific Gravity Values of Specimens

Compaction	No. Of Cycles	Bulk S.G
70-75 KN	8	2.32-2.35
80-85 KN	10	2.38 – 2.385
85-90 KN	12	2.395-2.41
RIDOT Standard	75 Blows/Side	2.40

The bulk specific gravity test was performed as soon as the compacted specimens cooled to room temperature. This test was performed according to ASTM D2726, Bulk Specific Gravity of Compacted Bituminous Mixtures using saturated surface dry specimens. The samples were first weighed in air (W_A), allowed to soak in water for 3 minutes and then weighed submerged in water (W_B). The samples were then removed from water, blotted dry and weighed in air (W_C). Using these values the bulk specific gravity was determined using the formula,

$$G_{mb} = W_A / (W_B - W_C) \tag{2-1}$$

Next, the specific gravity of the specimen was found using the standard ASTM test. The theoretical maximum specific gravity is determined using the procedure ASTM D 2041. Using theses values the air voids were calculated and determined to be 4.1%. The value recommended by RIDOT was specified between 4.0-4.5%.

2.4. Indirect Tension Testing on Asphalt Material

Indirect tension testing was performed on the asphalt material in order to calculate the tensile strength of the prepared sample material. The standard specimen geometry was obtained by taking a 4inch core from the rectangular specimen by using a coring machine. This produced a properly sized sample for the test as specified by ASTM C 496-96. The results were then compared with the standard Marshall specimen and were found to be in the same range. From standard elasticity theory (Sadd, 2005), a disk subjected to a point compressive loading, as shown in Fig 2.3 develops tensile stresses along the center plane given by,

$$\begin{aligned} \sigma_x(0,y) &= \frac{2P}{\pi D t} \\ \sigma_y(0,y) &= \frac{2P}{\pi D t}\left[\frac{D^2}{y(D-y)} - 1\right] \end{aligned} \tag{2-2}$$

where P is the applied load, t is sample thickness and D is specimen diameter as shown in Fig 2.3. The uniform stress relation for σ_x can then be used to determine the tensile strength of the material. Using the calibration chart, the proving ring in the tester was used to determine the

applied loading at failure, and relation $(2.2)_1$ was then used to determine the material tensile strength. IDT results are shown in the Table 2.3. The average splitting stress was found to be 0.64MPa.

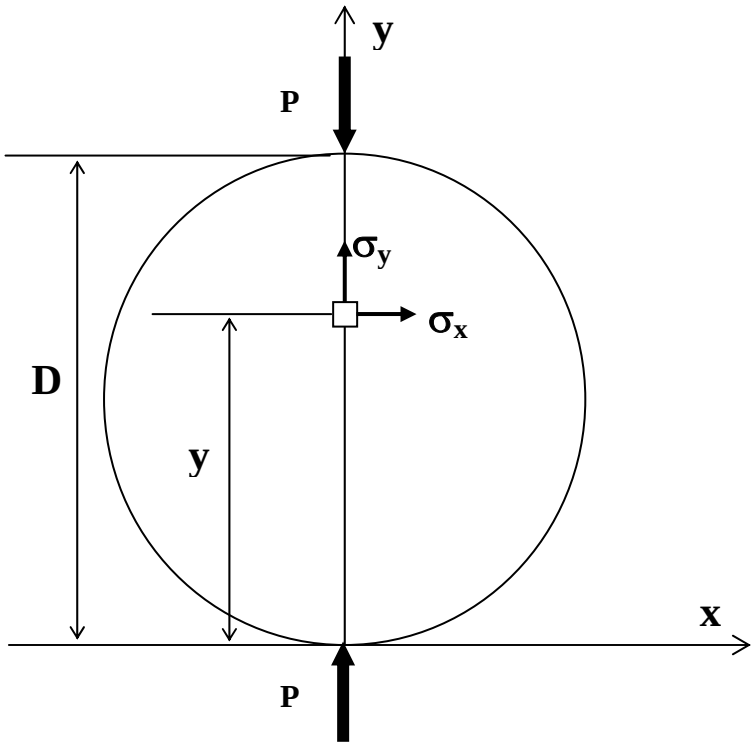

Fig. 2.3. IDT Load Geometry

Table 2.3. Experimental Results Obtained from Indirect Tension Tests

Test No.	Failure Load		Failure Splitting Stress	
	N	lb	MPa	psi
IDT1	7037.7	1583.5	0.69	100.1
IDT 2	6584.9	1481.6	0.65	94.3
IDT 3	6764	1521.9	0.67	97.2
IDT 4	6651.3	1496.5	0.66	95.7
IDT 5	6529.1	1469.0	0.64	92.8
IDT 6	6208.8	1397.0	0.6	87.0
IDT 7	5924.1	1332.9	0.59	85.6
IDT 8	6124.7	1378.1	0.6	87.0
Average			0.64	92.5
Std. Deviation			0.037	5.0
95% Confidence			0.026	3.5

2.5 Composite Asphalt/Concrete Block Sample Preparation

Once the asphalt portion of the block sample was prepared, it was placed in a specially designed mold that allowed concrete to be poured into the remaining volume to create the final composite sample, as shown in Fig. 2.4. It was suggested by RIDOT staff that the asphalt interface receive a saw cut to eliminate surface variability and to improve bonding with the poured concrete. Before pouring, Teflon tape was placed on the interface to create a stress free crack of desired position and length. Both central and edge interface cracks were created, as shown in Fig. 2.5; however, most of the experimental testing focused on central crack samples.

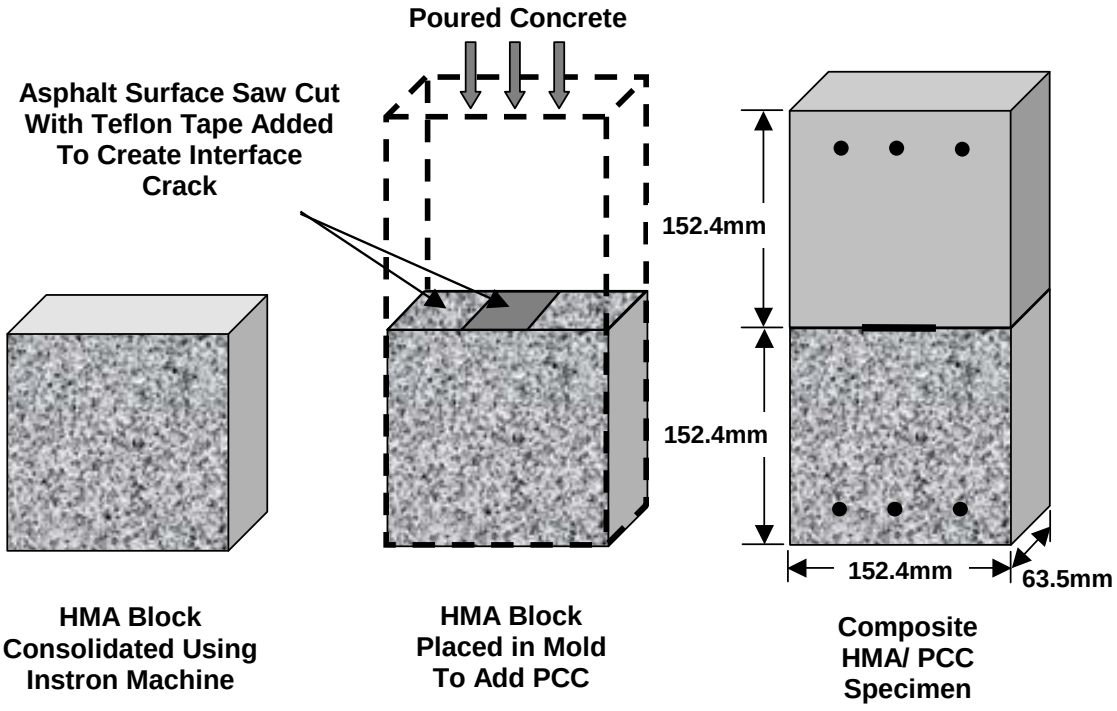

Fig. 2.4 Procedural Steps To Create Composite HMA/PCC Specimen With Central Interface Crack

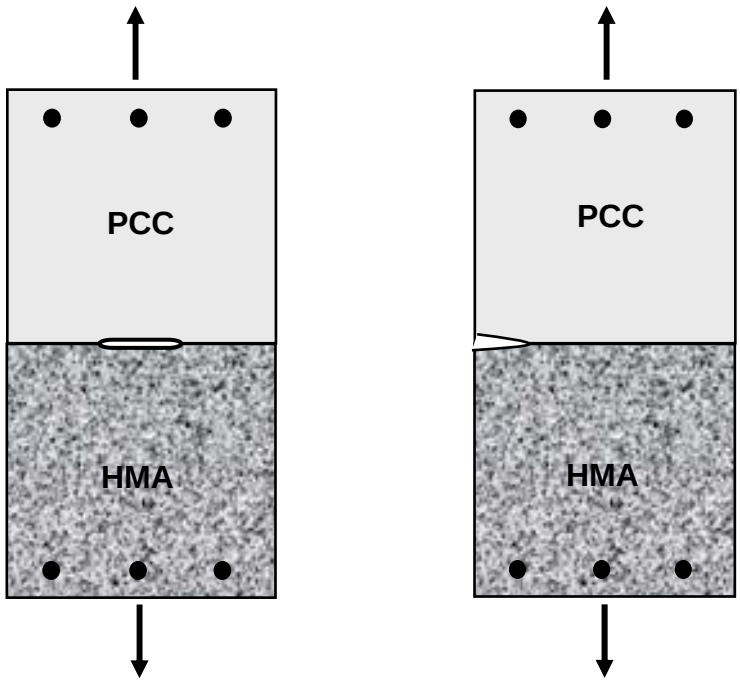

Fig.2.5 Rectangular Block Sample Geometries

The composite block samples were completed by first placing the rectangular asphalt portion in a wooden mold as shown in Fig 2.6 (a). The concrete was then poured over the asphalt specimen as shown in the Fig 2.6 (b). The mold was removed after 24 hours and the sample's concrete portion was submerged in water bath. Fig 2.7 shows the final composite asphalt sample after drying.

(a) Wooden Mold Containing Asphalt Sample

(b) Concrete Filled Mold

Fig. 2.6 Adding Concrete to Block Samples

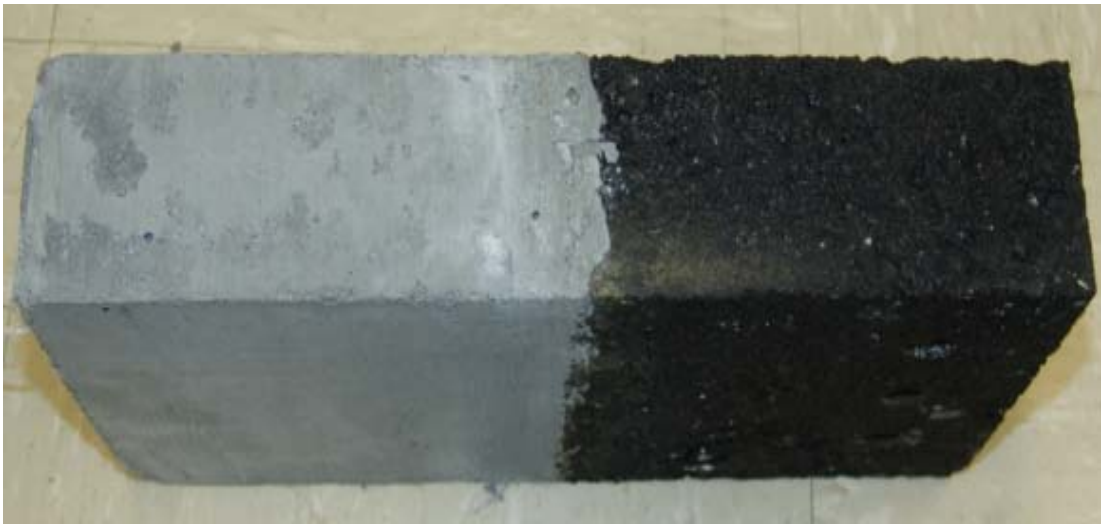

Fig. 2.7 Final Composite Rectangular Sample

2.6 Portland Cement Concrete Mix-Design

The Portland Cement Concrete mix design and mix proportion was Class WT (AE) a standard specification given by RIDOT. The specification details of the concrete mix are described below. The liquid admixtures and synthetic fibers were obtained from Grace Inc.

Total Cementitious(includes cement and mineral admixture)	705#/cy. (min)
Water/Cementitious Ratio	0.40 (max)
Corrosion Inhibitor	4.0 gals./cy.
Synthetic Structural Fiber Reinforcement	3.5 #'s/cy.
Mineral Admixture (fly ash) of total cement by weight	20 %
Slump Range (with fibers)*	2" – 4"
Air Content	6.5 % (± 1.5%)
Compressive Strength	
48 hours	3000 psi (Min.)
28 day	5000 psi (Min.)

* Maximum slump may be increased to 6" when ASTM C494 Type F high range water reducers are used.

Table 2.4 gives the concrete mix-design followed in the sample preparation with quantities adjusted according to the required proportion of the sample size.

Table 2.4. Concrete Mix-Design

Component	**Quantity Per Cubic Yard**
Portland Cement Type II	564 Pounds
Coarse Aggregate (3/4")	1700 Pounds
Fine Aggregate	1200 Pounds
Pozzolan (Ggbfs)	141 Pounds
Water	33.5 Gallons
Calcium Nitrite Corrosion Inhibitor	4 Gallons
Structural Fibers	3.5 Pounds
Air Entrainment	0.85 Ounces/100 Pounds Of Cement
High Range Superplasticizer	3.5 Ounces/100 Pounds Of Cement
Mid Range Superplasticizer	5.4 Ounces/100 Pounds Of Cement
Specified Air Content Range	6.5%±1.5%
Specified Slump Range	3"-6"

Further qualifications on the concrete mix design include the following material specifications:

- Portland cement: Type II
- Synthetic Structural Fiber Reinforcement

  The fibers are used to stop the non-structural cracks, increase abrasion resistance, and decrease concrete permeability. They can also disperse throughout the concrete, resist rust and corrosion and are safe to use. A synthetic structural fiber complying with the following requirements was added to the concrete:

  - Synthetic structural fibers shall meet the requirements of ASTM C 1116, Type III.
  - Synthetic structural fibers shall be monofilament, made of polypropylene or polypropylene/polyethylene blend with a specific gravity of 0.92.
  - Synthetic structural fibers shall have a minimum length of 1.5" (38 mm).
  - Synthetic structural fibers shall have an aspect ratio between 80 and 100.

- Water is required in the mixture for two purposes:
  - To react chemically with the cement and cause it to harden.
  - To make the mix plastic or workable enough to be used as intended.
- Liquid Admixture:
  - Corrosion Inhibitor – Calcium Nitrite based corrosion inhibitor conforming to Special Provision 605. These Chemicals provide protection for reinforcing steel in concrete exposed to salts from deicing chemicals and seawater.
- Superplasticizers:
  - The main action of the long molecules is to wrap themselves around the cement particles and give them a highly negative charge so that they repel each other. Produce concrete with high workability or concrete with high strength.

Coarse and fine aggregate and cement were all added to the cement mixer and were then pre-mixed prior to adding water. Once the cement-aggregate mixture was uniform, a combination of water and admixture was then added. When the batch had a uniform consistency the mixer was shutoff and the batch was poured into a wheelbarrow.

2.7 Basic Tests on Concrete Sample Material

Slump Test

A slump cone was dampened with a thin layer of water and then placed on a metal sheet. Concrete was placed into the cone in 3 equal volumes to fill the cone. Each equal volume of concrete was rodded 25 times with a 5/8" tamping rod. With a steady motion, taking approximately 7 seconds to lift the mold off the concrete, the cone was removed from the sample. A rod was then placed on the top surface of the cone that extended directly over the top of the sample as shown in the Fig 2.8. The difference in height between the cone mold and the sample was recorded using a ruler as shown. The slump was found to be 3" (76.2mm), which was in the range specified by RIDOT.

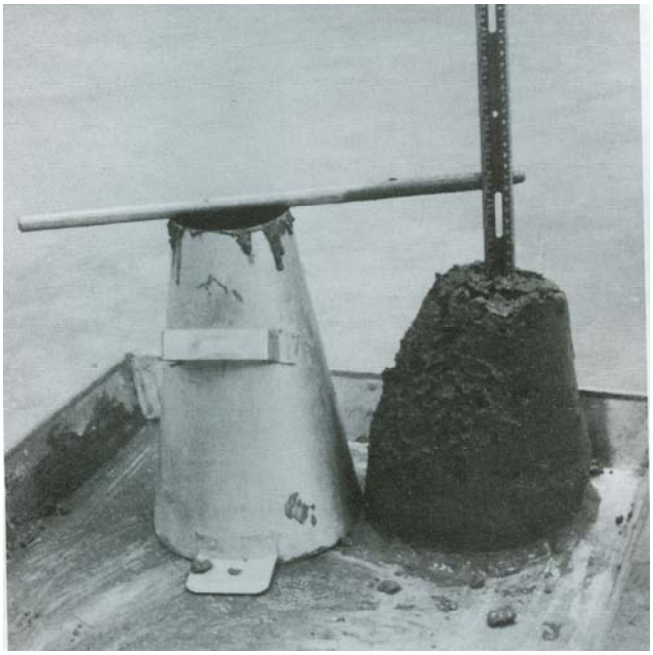

Fig. 2.8. Slump Test

Air Content Test

The procedure for finding air content of concrete used a pressure type air meter shown in Fig. 2.9. The air meter mold was filled with concrete and the air content was measured by the pressure method. Air content was found to be 4.8% and this was in the range specified by RIDOT.

Fig. 2.9. Pressure Type Air Meter

Compression Test

In order to determine the compressive strength of the concrete, compression tests were conducted on standard cylindrical samples of diameter = 4" and height = 8". A series of tests were done following the standard ASTM C 39-94 procedure and the compressive strength is given in the Table 2.5. Fig 2.10 shows the compressive strength attained with respect to the curing days.

Table 2.5 Compression Test Results

Sample No.	Load		Comp. Strength	
	kN	klb	MPa	psi
1 (7 days curing)	202.3	45.5	24.97	3621.6
2 (14 days curing)	285.8	64.3	35.16	5099.5
3 (21 days curing)	360.3	81.1	44.12	6399.1
4 (28 days curing)	444.8	100.1	54.81	7949.5
5 (28 days curing)	442.6	99.6	54.57	7914.7

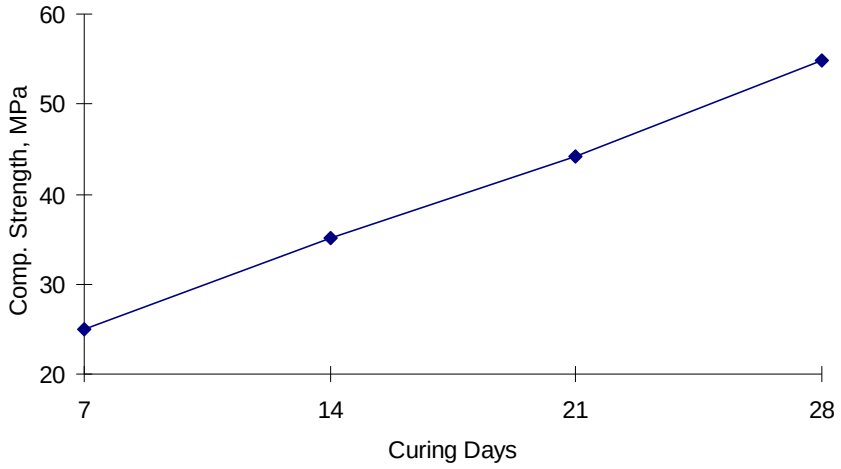

Fig. 2.10 Compression Test Results

2.8 Lap Joint Sample Preparation

The research program was also interested in the dynamic response of asphalt/concrete interface failure. In order to study such behavior, modification to our original block specimen geometry was required. With the desire to use a Split Hopkinson Pressure Bar (SHPB) apparatus, it was decided to limit our investigation to lap joint samples tested under shear loading. The geometry for these studies, shown in Fig. 2.1, consisted of a composite asphalt-concrete sample of cylindrical shape with an interface lying along the loading axis. In this fashion, bending effects would be minimized. The diameter of the lap joint sample was required to be slightly less than the SHPB bar size of 2" (50.8mm). Because of the limited interface area, no interface crack was introduced in these samples. Again an extensive preparation process was followed to construct such specimens.

Material for the asphalt portion of these samples was first prepared using a superpave gyratory compactor that produced a 6'' diameter cylindrical sample of proper compaction. As shown in Fig. 2.11, this sample was then cored to collect smaller cylinders for the lap joint specimens. A coring machine with a bit of 1.75" (45mm) was used for coring asphalt samples. This sub sample was then saw cut both axially and half cross-sectioned to create the necessary match for the concrete portion as shown in the Fig 2.12.

Fig. 2.11 Cylindrical Asphalt Sample Used to Sub Sample to Extract Cores for Lap Joint Samples

Fig. 2.12 Sectioned Asphalt Sample Portion

Once the asphalt portion was completed, it was then placed into a special cylindrical mold that would allow for proper concrete pouring and forming (see Figure 2.13). Removable semi-circular plugs were placed on the asphalt sample to provide required open space between the asphalt and concrete thereby guaranteeing that the axial compressive end loading would be transmitted only to the interface. Identical concrete mix as discussed previously in Section 2.6 was also used for these specimens, and Fig. 2.14 illustrates the mold when filled with concrete. The mold was removed after 24 hrs and the spacer plugs were also detached. The sample was then cured for a minimum of 7 days. The final composite lap joint sample coming from this process is shown in Fig 2.15, and a cutout of 0.25" (6mm) was made at each end of the joining surface to ensure sample end loading is transferred to shear along the asphalt-concrete interface.

Fig. 2.13 Cylindrical Mold with Asphalt Portion Just Prior to Concrete Pouring

Fig. 2.14 Mold Filled with Concrete to form Composite Lap Joint Sample

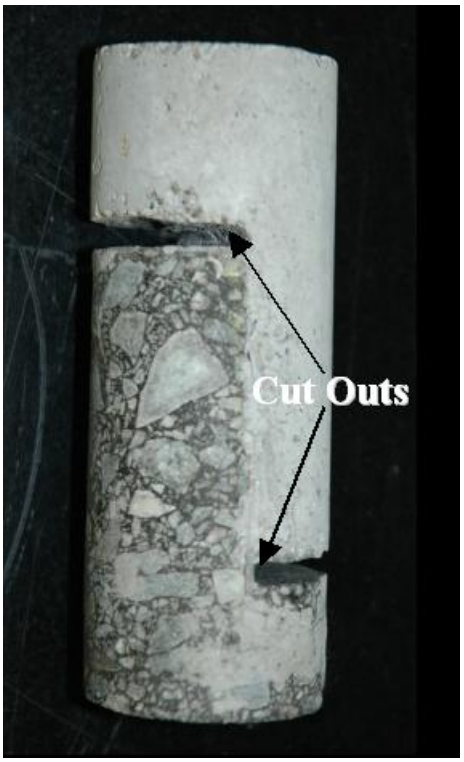

Fig. 2.15 Composite Lap Joint Sample with Cutouts

CHAPTER III – QUASI-STATIC BIMATERIAL CHARACTERIZATION TESTING

3.1 Introduction

This chapter describes the quasi-static testing and analysis of the composite block samples previously discussed in Section 2.5. The program included laboratory samples with central and edge cracks and also samples with no initial cracks. We also tested a limited number of block specimens taken from roadway cores. The goal of this effort was to characterize the interfacial failure between the concrete and asphalt under static loading conditions that included both tensile and shear loadings that would simulate particular traffic loading scenarios. The focus was primarily concerned with evaluating the failure within the context of fracture mechanics theory and we also conducted a preliminary finite element analysis of the sample.

3.2 Interfacial Fracture Mechanics

We wish to apply linear elastic fracture mechanics theory (LEFM) to the interfacial failure of the concrete/asphalt interface. Within this theory, three fundamental modes of fracture failure are identified, and these are shown schematically in Fig. 3.1. Mode I is referred to as opening mode and is the most common form of crack propagation. Modes II and III are shearing modes that would allow for crack propagation due to material displacements along (parallel to) the crack plane. As will be shown later, for an interface crack between dissimilar materials both both modes I and II are intrinsically present in such a deformation problem.

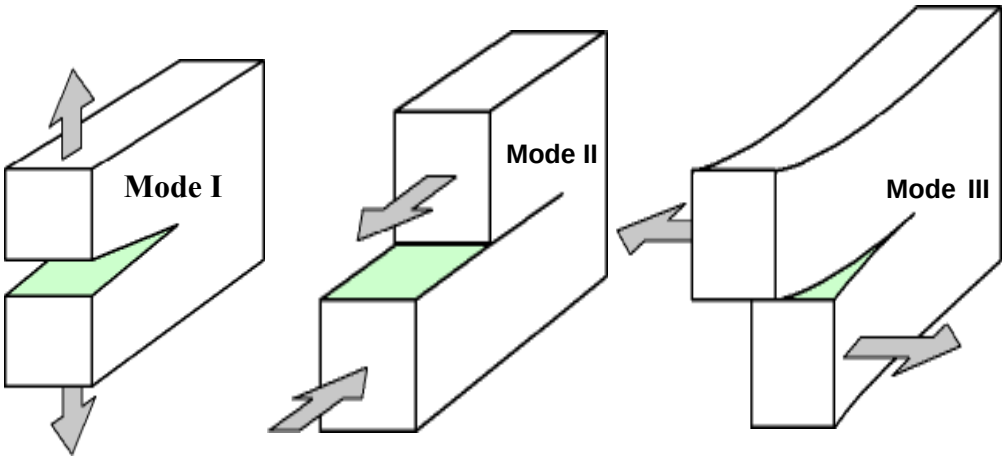

Fig. 3.1. Three Modes of Crack Propagation

Of fundamental importance in fracture mechanics theory is the local stress distribution around the crack tip. From elasticity theory (Sadd, 2005), it can shown that the stresses will be unbounded (singular) at this location. For a two-dimensional case, the general form of such stress fields can be expressed as

$$\sigma_{ij} = \frac{K}{\sqrt{2\pi r}} f_{ij}(\theta) \tag{3.1}$$

where r and θ are the radial and angular coordinates measured from the crack tip, f_{ij} is a specified distribution function that depends only on the angular coordinate, and K is a parameter called the *stress intensity factor* that specifies the intensity of the singular stress state near the crack tip. At failure, K is referred to as the critical stress intensity factor K_c, and this has been shown to be related to the *fracture toughness* of the material. High values of K_c would indicate a material that has high resistance to fracture failure.

Of interest in the current study is the application of LEFM to the interfacial crack problem. Previous research has been done on this problem, and solutions for the stress distribution around the tip of a crack lying along the interface between two dissimilar materials has been developed for idealized loading geometries. Examples of this previous work include: Williams (1957, 1959), Hutchinson et al. (1987), Rice (1988), Comninou (1990), Rice, Suo, and Wang (1990). These studies typically developed two-dimensional solutions for the local stress fields and provided relations to determine the corresponding stress intensity factors for mode I and II crack propagation in terms of far-field loading. In particular, Hutchinson et al. (1987) and Rice (1988) have developed such solutions for the bimaterial system of an interface crack in an infinite medium with uniform far-field stress as shown Fig. 3.2.

For this problem, the crack tip stress field can be characterized by a complex stress intensity factor of the form given by

$$K = K_1 + iK_2 = \left(\sigma_y^{\infty} + i\tau_{xy}^{\infty}\right)(1 + 2i\varepsilon)(\pi L/2)^{1/2} L^{-i\varepsilon} \tag{3.2}$$

where K_1 and K_2 are the mode I and mode II stress intensity factors, L is the crack length, and the material properties are accounted for within the *mismatch parameter*,

$$\varepsilon = \frac{1}{2\pi} \ln\left(\frac{\frac{x_1}{\mu_1} + \frac{1}{\mu_2}}{\frac{x_2}{\mu_2} + \frac{1}{\mu_1}}\right), \quad x_i = 3 - 4\nu_i \text{ (Plane Strain)} \tag{3.3}$$

where μ_i are the shear moduli, and υ_i are the Poisson ratios of each material. Note that the loading angle ψ in Fig. 3.2, would also serve as a crack orientation angle for a crack oriented at angle ψ from the horizontal direction.

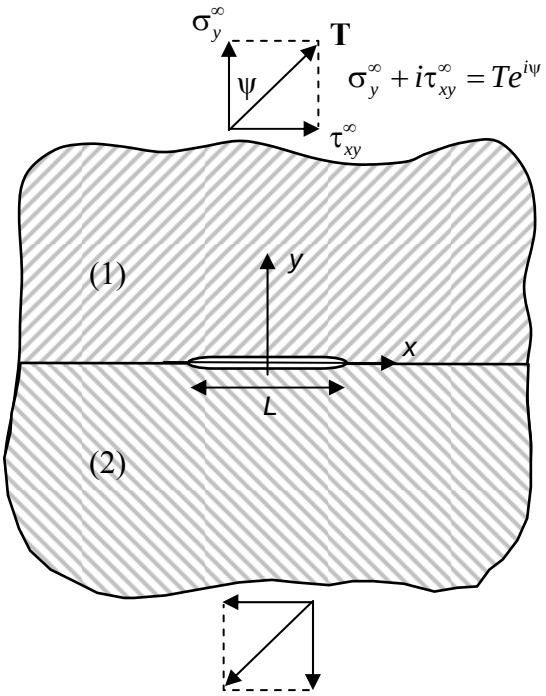

Fig. 3.2. Interface Crack in an Infinite Medium.

Note that for the special case of vertical tension (no far-field shear loading and with $\psi = 0$), relation (3.2) gives the mode I and II stress intensity factors as

$$\begin{aligned} K_1 &= \sigma_{yy}^\infty \sqrt{\pi L/2}\left[\cos(\varepsilon \ln L) + 2\varepsilon \sin(\varepsilon \ln L)\right] \\ K_2 &= \sigma_{yy}^\infty \sqrt{\pi L/2}\left[2\varepsilon \cos(\varepsilon \ln L) - \sin(\varepsilon \ln L)\right] \end{aligned} \tag{3.4}$$

Using relation (3.2), the variation of K_1 and K_2 with interface angle ψ can be determined. These results are shown in Fig. 3.3 for the case of unit loading ($T = 1$) using typical elastic moduli for asphalt and concrete given in the caption. The shear moduli needed in relatation (3.3) was calculated using the standard elasticity relation $\mu = E/(2(1+\nu))$. It can be seen that K_1 generally decreases while K_2 increases with orientation angle. Note also that because of the

material mismatch, K_2 does not vanish at $\psi = 0$. This relation can be used to determine the stress intensity at failure load and thereby determine the interface fracture toughness.

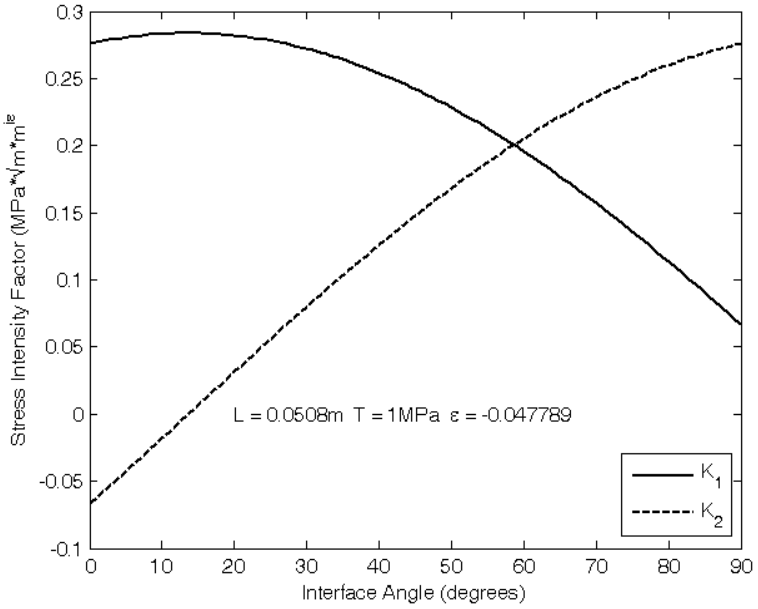

Fig. 3.3 Stress Intensity Factors vs Orientation Angle for Interface Crack.
(E_c = 34GPa, E_a = 4.9GPa, ν_c = 0.2, ν_a = 0.35)

As shown in Fig. 3.4, results for far field loading at the angle ψ is equivalent to vertical loading applied to a sample with the interface crack oriented at the same angle with respect to the horizontal plane. This concept will later be used for some of our sample testing.

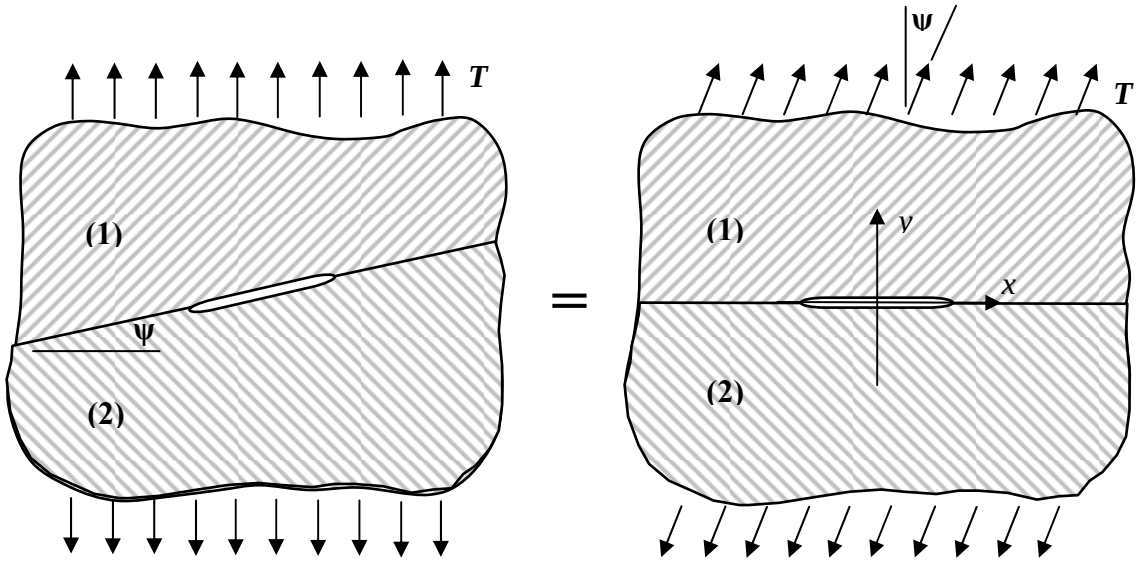

Fig. 3.4. Equivalency of Inclined Loadings

3.3 Uniaxial Tension Testing of Composite Block Samples With Normal Interface

A series of experiments were conducted on composite block samples using an interfacial center crack of length 2" (50mm) with the interface oriented normal to the loading direction, as shown in Fig. 3.5. Such rectangular block samples are normally used in this type of fracture mechanics testing. Special fixturing was required to properly load the specimen in the testing machine, as shown in Fig. 3.6. Appropriate far field uniform tensile loading was applied through the bolted bearing plates as shown. These steel loading plates had a rough inside sand paper surface to provide sufficient friction to achieve uniform sample loading.

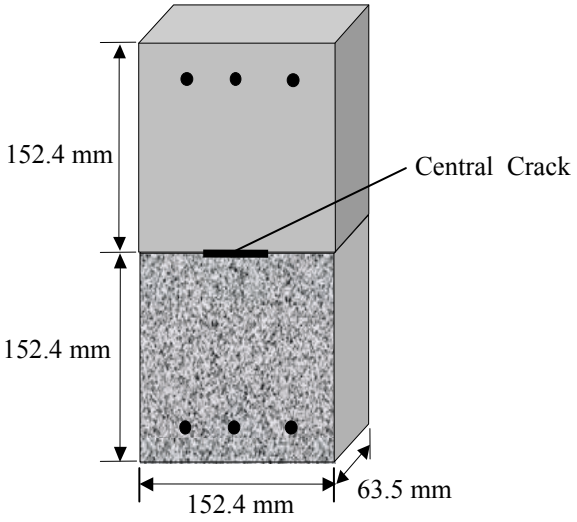

Fig. 3.5 Composite Asphalt-Concrete Specimen Geometry With Central Interface Crack and Normal Loading

Fig. 3.6 Sample in Testing Machine

Seven samples were tested at room temperature (70^{o}F) using this configuration and a typical load-extension curve obtained from one test is shown in Fig 3.7. Peak loads obtained from this load-extension data were used in calculating the stress intensity factors K_1 and K_2 using relations (3.4). As shown in Fig. 3.8, failure initiated at the initial interface crack. However, crack propagation normally did not follow along the bi-material interface, and the failure crack path generally propagated in the asphalt material a few millimeters from the interface. This type of behavior would suggest that the interface is somewhat stronger than the nearby asphalt

material and it is also apparent that the granular nature of asphalt contributes to the irregular failure patterns. Fig. 3.9 shows a post-mortem photograph of a typical failure surface from the concrete side of the sample. At room temperature, asphalt has considerable inelastic behavior thereby producing a failure surface with asphalt binder pullout resulting from local inelastic flow deformation between aggregate particles.

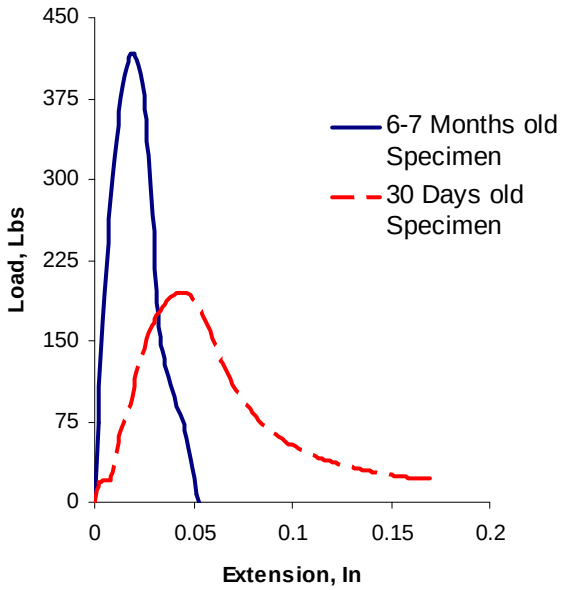

Fig. 3.7 Load Extension Behavior for Central Crack Sample with Normal Interface.

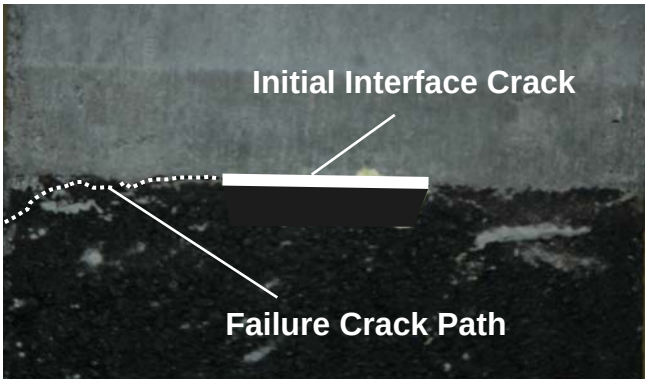

Fig. 3.8 Interface Crack Path 30-Day-Old Sample.

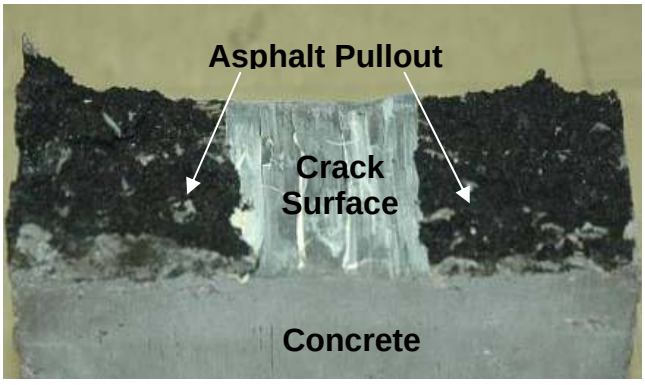

Fig. 3.9. Sample Post Mortem Failure (30-Day-Old) Sample

Stress and stress intensity factor results obtained from this series of tests are shown in Table 3.1. Collected data indicates that failure occurred at lower loads for 30-day-old asphalt samples when compared to 180-200-day-old samples. Also it was observed that the failure crack propagation path was closer to the interface for older asphalt material. These results indicate an extremely low value for a bimaterial interface. Using standard three-point bend tests, the K_{1c} value for 30-35 day-old asphalt was found to be 0.075 MPa$\sqrt{m}$. K_{1c} values for concrete were found in the literature in the range between 1.2-1.8 MPa$\sqrt{m}$. Results shown in Table 3.1 indicate that interface fracture toughness values were found to be less than the corresponding homogeneous materials. Similar results have been observed in other research done on different bimaterials, see for example McBride et al. (2002) where the fracture toughness of an Aluminum Silicate-Cement interface was K_{1c}=0.068Mpa-m$^{1/2}$ and K_{2c}=0.002Mpa-m$^{1/2}$ both values below the individual homogeneous material fracture toughnesses.

Table 3.1 Uniaxial Test Results – Normal Interface

Test No.	**Failure Load, N**	**Average Far-Field Stress (kPa)**	**Average Interface Stress (kPa)**	**K_1 (MPa $\sqrt{m}$)**	**K_2 (MPa$\sqrt{m}$)**
30 Day Old Samples					
FS1	818	84.6	126.8	0.022	0.0088
FS2	866	89.6	134.3	0.023	0.0094
FS3	943	97.6	146.2	0.025	0.0102
			Average	0.024	0.0094
			Standard Deviation	0.0017	0.0007
			95% Confidence	0.0019	0.0008
180-200 Day Old Samples					
FS4	1846	193.1	286.2	0.051	0.020
FS5	2100	217.2	325.6	0.058	0.023
FS6	2255	234.4	349.6	0.062	0.025
			Average	0.057	0.022
			Standard Deviation	0.0055	0.0025
			95% Confidence	0.0063	0.0028

3.4 Uniaxial Tension Testing of Composite Block Samples With Inclined Interface (Mixed Mode)

Since starting and stopping traffic will generate substantial shear loading to the concrete/asphalt interface, it was decided to also test composite samples under more mixed mode loading with a significant shear component along the interface. This was accomplished by constructing samples with the interface (and crack) oriented at an angle with respect to the loading direction, see Fig. 3.4. The specimen geometry was again a rectangular block of identical outside dimensions as used previously (Fig. 3.5). Preparation procedures were the same as described in Section 2.5, and the asphalt material was 60 day-old. The interface was inclined to the loading direction by $\psi = 30°$ and contained an initial central crack of length 2" (50mm), see Fig.3.10. Samples were tested under quasi-static tension thereby producing a mix-mode loading to the interface crack. Typical load-extension behavior for these specimens is shown in Fig. 3.11. Comparing this response with the corresponding behavior for the normal interface (Fig. 3.7), indicates that samples under mixed mode loading exhibit smaller deformation.

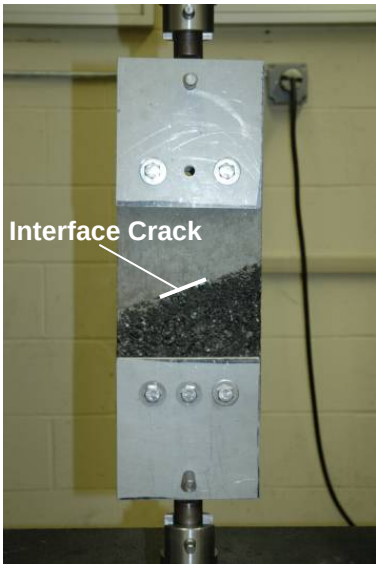

Fig. 3.10. Composite Sample Under Mixed-Mode Loading.

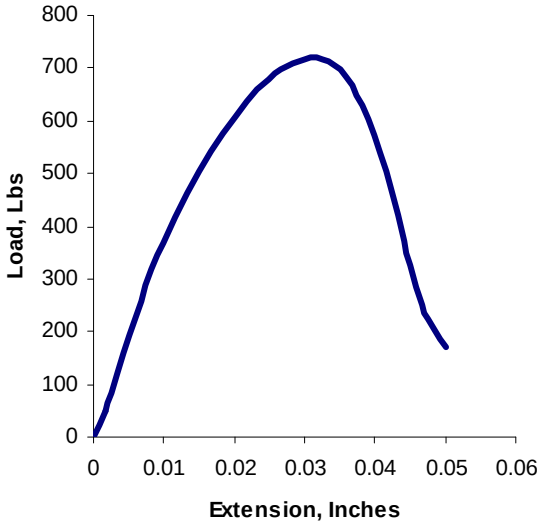

Fig. 3.11. Load Extension Curve Mixed-Mode Sample

Mixed mode stress intensity factor results obtained from these individual tests, along with average, standard deviation and 95% confidence are provided in Table 3.2. It was found that the failure load and resulting stress intensity factors for samples with an inclined interface were

higher than normal interface test results. It would seem that mode mixity (decrease in normal stress and increase in shear stress) is the primary reason for such increase in the K_1 and K_2 values compared to the straight interface. Figure 3.12 illustrates that for mixed mode samples, the first failure crack propagation tends to be somewhat closer to the interface. The secondary crack path propagates more in to the asphalt material because the specimen is not symmetric about the vertical centerline and edge effects will cause the crack to move away from the interface. A post mortem photograph of a typical failed sample is shown in Fig. 3.13. As previously observed in Fig. 3.9, the interface asphalt has exhibited considerable inelastic behavior thereby producing a failure surface with asphalt binder pullout resulting from local inelastic flow deformation between aggregate particles.

Table 3.2 Results For Mixed Mode Tension Tests

Test No.	**Failure Load, (N)**	**K_1 (MPa√m)**	**K_2 (MPa√m)**
30° inclined Interface			
I 1	3200	0.098	0.047
I 2	3385	0.1	0.051
I 3	3590	0.13	0.057
Average		0.109	0.051
Std. Deviation		0.017	0.05
95% Confidence		0.02	0.05

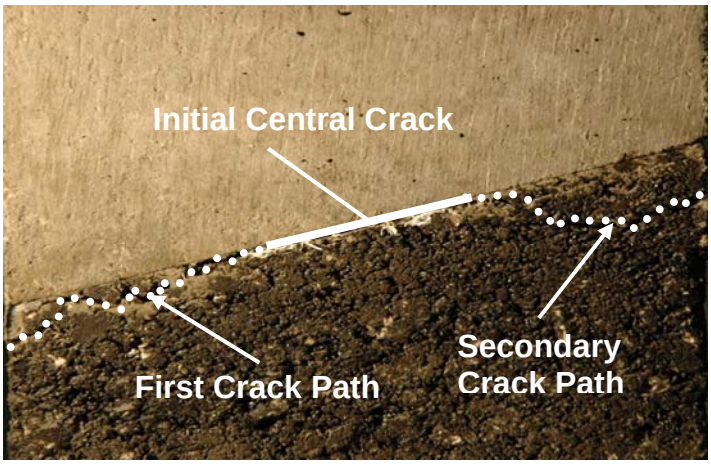

Fig. 3.12 Failure Crack Propagation in Mixed Mode Sample

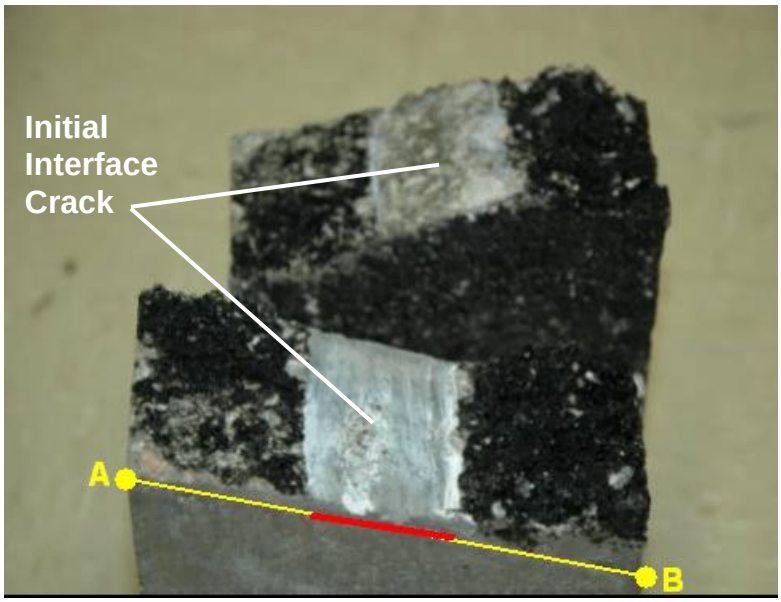

Fig. 3.13 Post Mortem Photograph Showing
Failure of Inclined Interface Sample

3.5 Core Sample Testing

Several core samples taken from the white topped pavement on Rte 116 in Lincoln, RI were provided by RIDOT personnel. Of the five or six cores provided, only three useable samples were obtained. The six inch cores were sub-sampled by using a diamond saw to cut out rectangular block sample geometries needed for the fracture interfacial-failure experiments. This step is shown in Fig. 3.14(a) with cutting along the axial direction. The final preparation procedure involved the use of URI's Water Jet Machining Facility to cut a central slit along the concrete/asphalt bond. The machined slit was then sharpened with a special hacksaw blade to more closely approximate an interface crack geometry similar to Fig. 3.5. The final sample product is then shown in Fig. 3.14(b).

Similar to the testing of our laboratory samples described in section 3.3, the core samples were tested in uniaxial tension using an Instron machine, see Fig. 3.15(a), under quasi-static loading (0.04 in/min head rate). In comparison to the laboratory samples, failure of these core samples was much more brittle-elastic with relatively little inelastic deformation along the concrete-asphalt interface, see Fig. 3.15(b). However, it was observed that the actual interface was not planar and contained numerous roughness textures, some as large as 0.3 in.

(a) Sub-Sampled Core

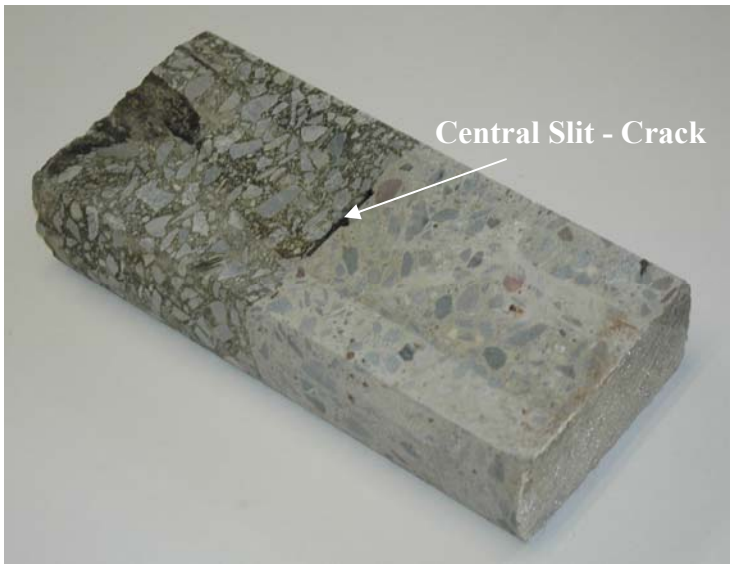

(b) Sample With Central Crack Cutout

Fig. 3.14 Sub-Sample Processing of Core Samples

(a) Core Sample in Testing Machine

(b) Core Sample Postmortem

Fig. 3.15 Core Sample Testing and Postmortem Analysis

Load-extension behaviors for each of three core samples are shown in Fig. 3.16, and mixed mode stress intensity factor results obtained from this data are given in Table 3.3. It is found that the failure loads and resulting critical stress intensity factors for the core samples were higher than those found in the laboratory sample test results shown in Table 3.1. This behavior follows the aging effects found in the laboratory sample data set. It is assumed that the core sample material taken from the roadway were several years old, while our laboratory specimens were only 1-6 months old. Summarizing this aging behavior, the average mode-I stress intensity factor K_I for samples of age: 1-month, 6-months and several years was found to be: 0.024, 0.057, and 0.069 MPa/√m, respectively.

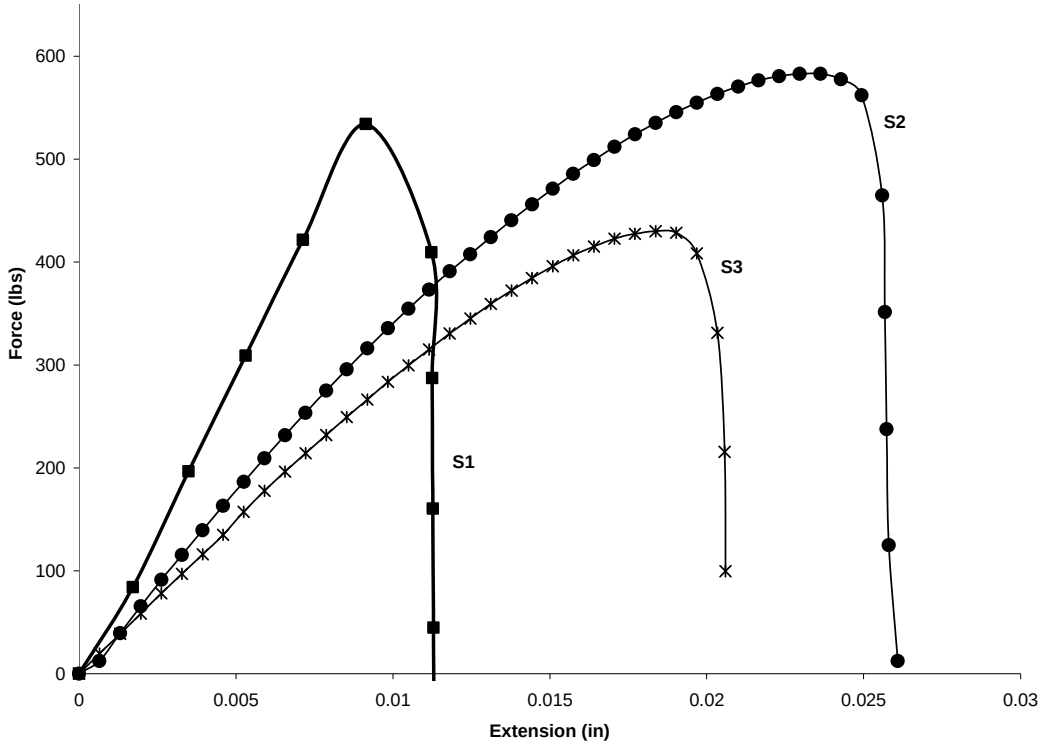

Fig. 3.16 Load Extension Results for Core Sample Tests

Table 3.3 Core Sample Tension Test Results

Test No.	Failure Load	Failure Stress (kPa)	Crack Length(mm)	K_1 (MPa√m)	K_2 (MPa√m)
S1	534(lb) 2376(N)	278.2	53	0.079	0.019
S2	583(lb) 2594(N)	259.4	47	0.069	0.017
S3	430(lb) 1913(N)	207.3	52	0.058	0.014
Average	2294(N)	248.3	50.67	0.069	0.017

3.6 Cohesive Zone Interface Modeling

Since the observed interfacial failure behavior between the concrete and asphalt showed considerable inelastic response, it was felt that perhaps a non-fracture mechanics approach might be used to model such behavior. Needlemen (1987) has previously presented a cohesive zone model based on the nucleation of voids from second phase particles (aggregates). This has been used to develop interfacial decohesion relations that predict the traction across an interface to exhibit increasing and decreasing behaviors similar to those shown in Figs. 3.7, 3.11 and 3.16. Based on this similarity, we explored the feasibility of using such a cohesive zone model to simulate the inelastic behavior of the concrete/asphalt interface.

Needleman's work developed a model for the normal and shear components of the interfacial tractions. The relation for the normal traction magnitude was given by

$$T_n = \frac{27}{4}\sigma_{\max}\left\{\left(\frac{u_n}{\delta}\right)\left[1-2\left(\frac{u_n}{\delta}\right)+\left(\frac{u_n}{\delta}\right)^2\right]+\alpha\left(\frac{u_t}{\delta}\right)^2\left[\left(\frac{u_n}{\delta}\right)-1\right]+\alpha\left(\frac{u_b}{\delta}\right)^2\left[\left(\frac{u_n}{\delta}\right)-1\right]\right\} \quad (3.5)$$

where u_n , u_t, u_b are the normal and shearing components of the interfacial displacement, $\sigma_{\max}$ is the maximum traction carried by the interface, δ is a characteristic length, and α specifies the ratio of shear to normal interface stiffness. Applying this model to our uniaxial tension sample shown in Fig. 3.6, we will make the simplifying assumptions that the shearing interfacial displacements can be neglected and that the normal displacement scales with the sample axial deformation. Under these assumptions the model should then be able to simulate the experimental data shown in Fig. 3.7. Using model parameters $\sigma_{\max} = 41 psi$, and δ = 0.05in, a

comparison of the cohesive zone model with the 6 month old material data is shown in Fig. 3.17. Based on the reasonably good comparison, it appears that this model could be useful in predicting the complex inelastic debonding behavior at the concrete/asphalt interface. Additional research would have to be done to further explore this issue in detail.

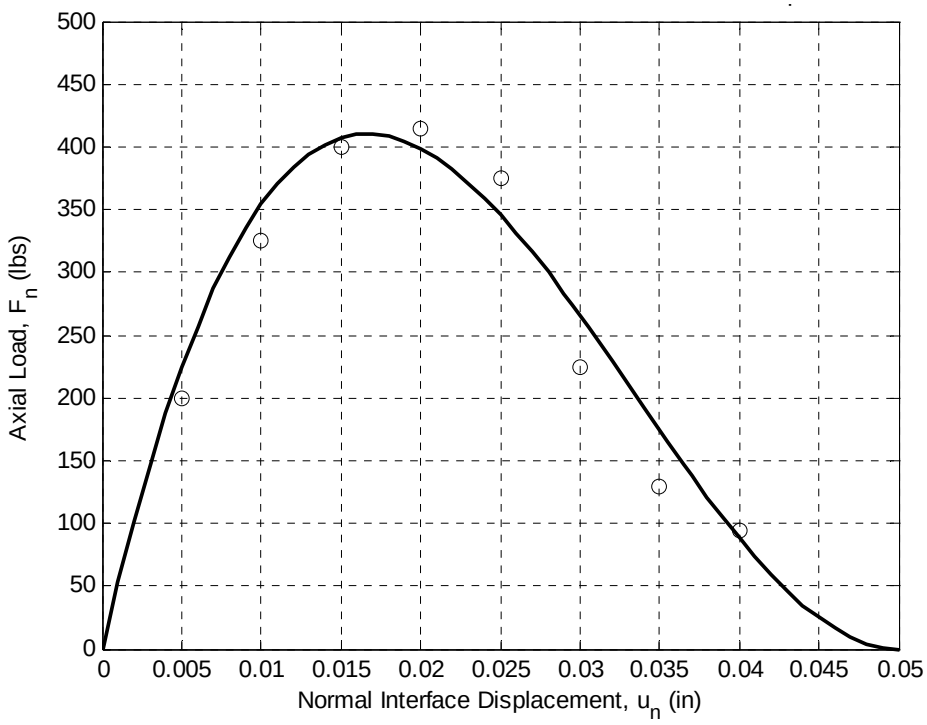

Fig. 3.17 Comparison of Cohesive Zone Model with Experimental 6-Month Old Material Data (Open Circles) from Fig. 3.7

CHAPTER IV – FINITE ELEMENT MODELING

4.1 Inroduction

In order to explore general details of the stress distribution in the vicinity of the concrete/asphalt interface crack, a finite element analysis (FEA) was conducted on the composite block sample. The FEA study used the well verified ABAQUS code, under the conditions of linear elastic behavior and incorporated three-dimensional brick elements. Although considerable inelastic deformation is observed at failure, the goal of this study was to determine the stress conditions just prior to interfacial failure. Models incorporating both center and edge cracks were developed.

4.2 Finite Element Model Development

The composite block sample geometry for the central crack case is again shown in Fig 4.1. ABAQUS provides convenient auto-meshing that enables the user to quickly develop suitable three-dimensional element meshes. For this type of model, we chose three dimensional brick elements for the discretization. The FEA model used interface gap elements along the concrete/asphalt interface. Although these gap elements could be used to simulate the local deformation mechanics of the bond, it was felt that this type of analysis was beyond the goals of the current study. Therefore the gap element stiffness was not varied, and a single high stiffness value (larger than either material) was chosen for all simulations. This then simulated the case of a perfectly bonded interface where the two materials at the interface move together. Of course over the crack surfaces, the adjacent nodes from each material side are allowed to be free and unconstrained. The boundary and loading conditions for the FEA model are shown in Fig. 4.2. A uniform load of 100 lb (444.8 N) was applied to the sample's top while at the bottom, the vertical displacement (U_3) was fixed and the other two displacements (U_1 and U_2) were unconstrained. It was felt that these conditions would serve to simulate the conditions that the sample would experience during testing in the Instron machine.

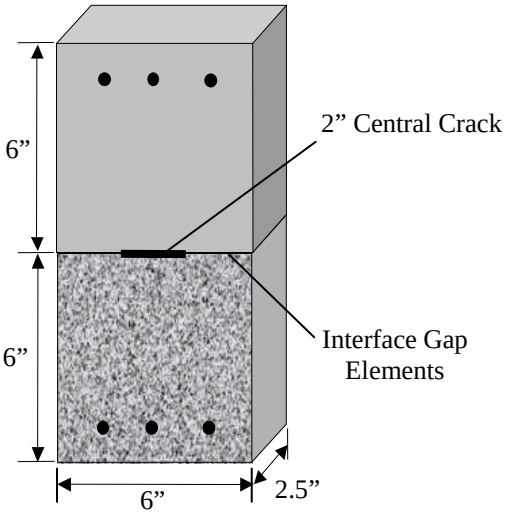

Fig. 4.1 Composite Asphalt-Concrete Specimen Geometry With Central Interface Crack

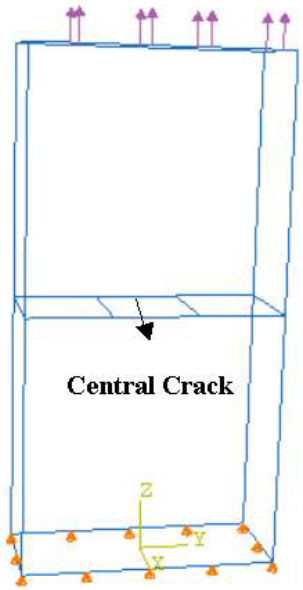

Fig. 4.2 FEA Central Crack Model

In the meshing process, we defined attributes and controls such as mesh density, element shape and element type, and thus generated appropriate meshes for the sample geometry. A bias seeding technique along an edge was used as shown in Fig. 4.3. For example, a bias ratio of 3, means the largest element on the edge will be three times the size of the smallest element. This ratio was used for element size distributions near the crack tip in our simulations. The scheme creates a finer mesh near the crack tip to help capture the high stress gradients while allowing for a more coarse mesh away from the crack, see Fig 4.4. The total number of elements generated in the overall model was 54,800.

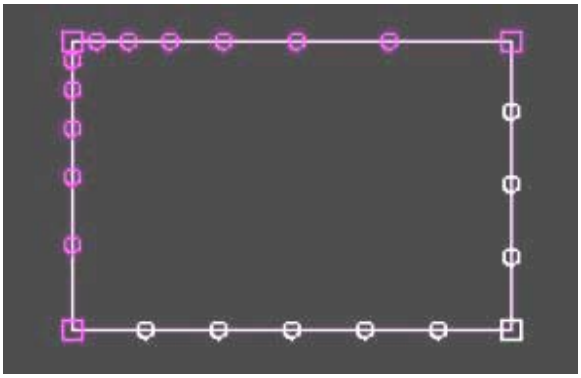

Fig. 4.3 FEA Model With Biased Seeding

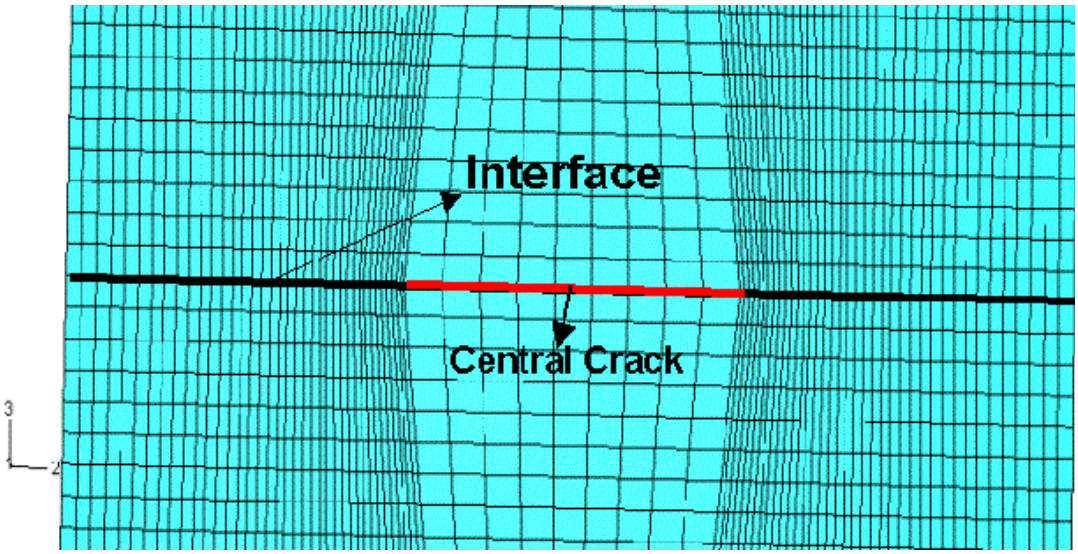

Fig. 4.4 Local View of Mesh Near the Crack

The finite element model used linear elastic analysis with material properties for concrete and asphalt given by: E_c = 34GPa, E_a = 4.9GPa, ν_c = 0.2, ν_a = 0.35.

4.3 FEA Results for Central Crack Geometry

FEA results for the vertical normal stress S_{33} distributions are shown in Fig. 4.5 for the complete sample and Figs. 4.6 and 4.7 show the results for asphalt and concrete separately.

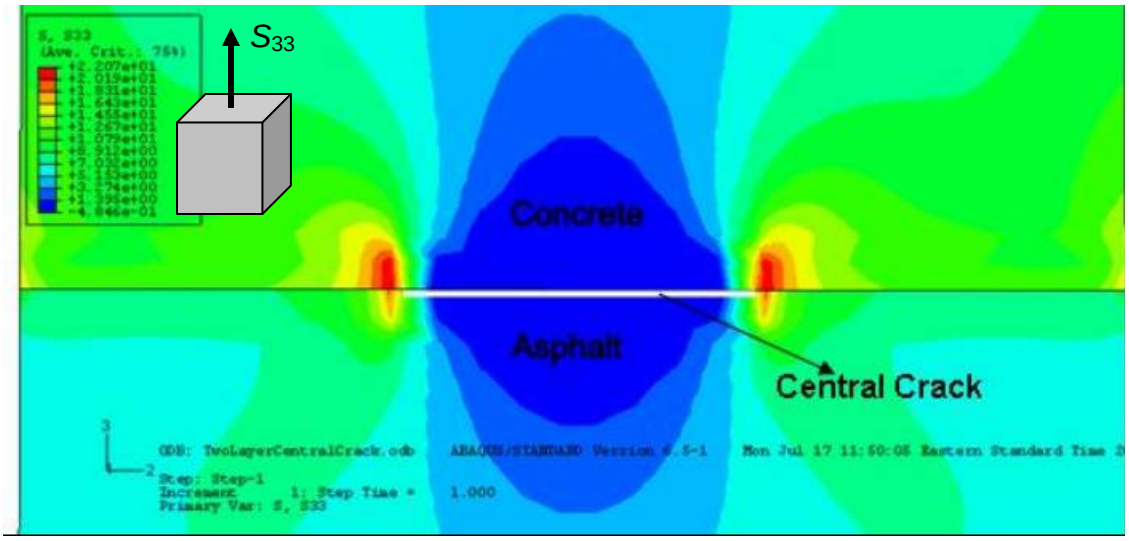

Fig. 4.5 Normal Stress Contours S_{33} for Composite Sample

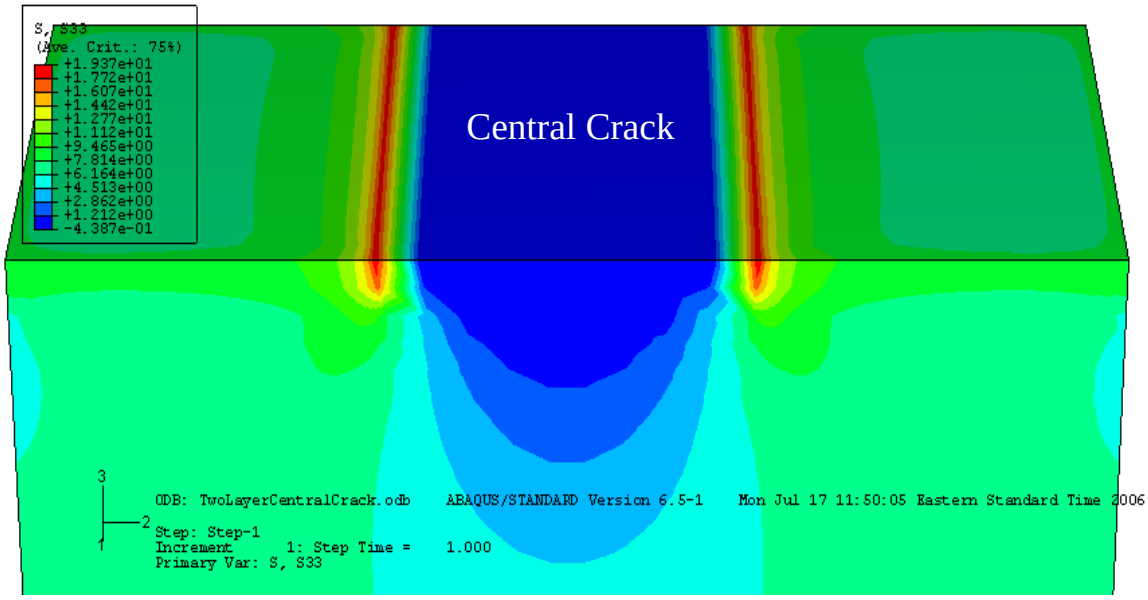

Fig. 4.6 Normal Stress Contours S_{33} for Asphalt Portion

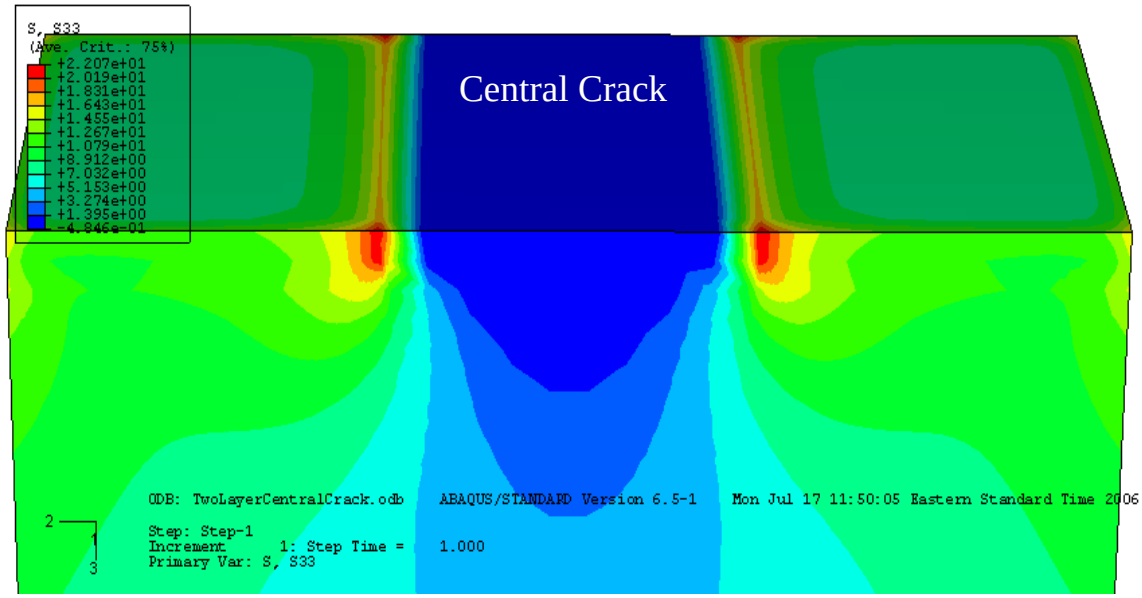

Fig. 4.7 Normal Stress Contours S_{33} for Concrete Portion

As expected the stress contours illustrate high stresses near the crack tips with a rapid decrease as we move away. Since the model matches the actual sample size, we can also see the edge effects near the right and left sides of the sample.

In order to explore in more detail the stress distribution along the interface, FEA results were collected at nodes along the interface directly in front of the crack. Comparisons have been

made between these FEA results and the analytical solution for the bimaterial interface crack problem given by Hutchinson et al. (1987) and Rice (1988). The far field stress σ_y^{∞} was added to the analytical result since the model is of finite size. Comparison results between theory and FEA predictions are shown in the Fig 4.8. The analytical solution rises to infinity at the crack tip while FEA simulation cannot predict such results. Since the analytical solution is valid only near the crack tip, it is expected that the comparisons will not be as good close to the sample's edge. However, in general the FEA results match reasonably well with the analytical solution.

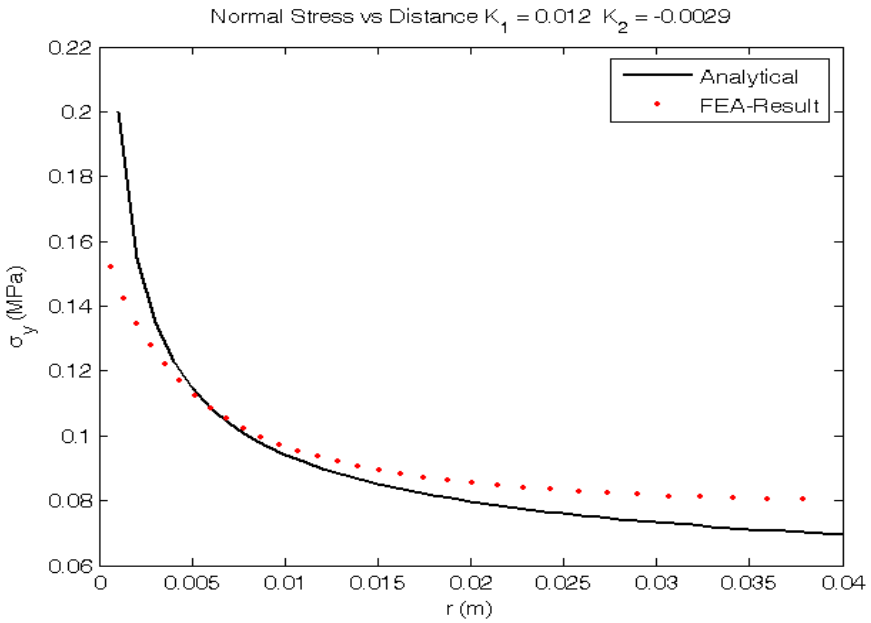

Fig. 4.8 Comparison of FEA and Analytical Normal Stress Distributions for Central Crack Sample

FEA shear stress S_{23} results are shown in Fig 4.9 for both the entire sample and the asphalt and concrete separately. Shear stress contours also shows high local stresses near the crack tip that the stress is very high near the crack tip. As done with normal stresses, the FEA shear stress results along the interface have been compared with the analytical solution given by Hutchinson et al. (1987) and Rice (1988). Comparison results are shown in the Fig 4.10, and it is observed that FEA results match near the crack tip but differ at points closer to the sample's edge. As previously mentioned this is to be expected since the analytical solution is not valid away from the crack tip.

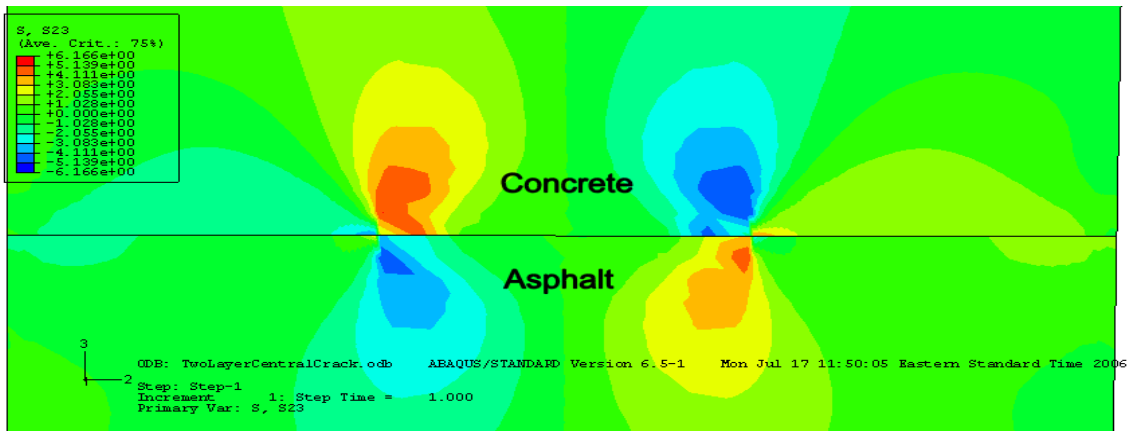

(Shear Stress Distribution for Composite Sample)

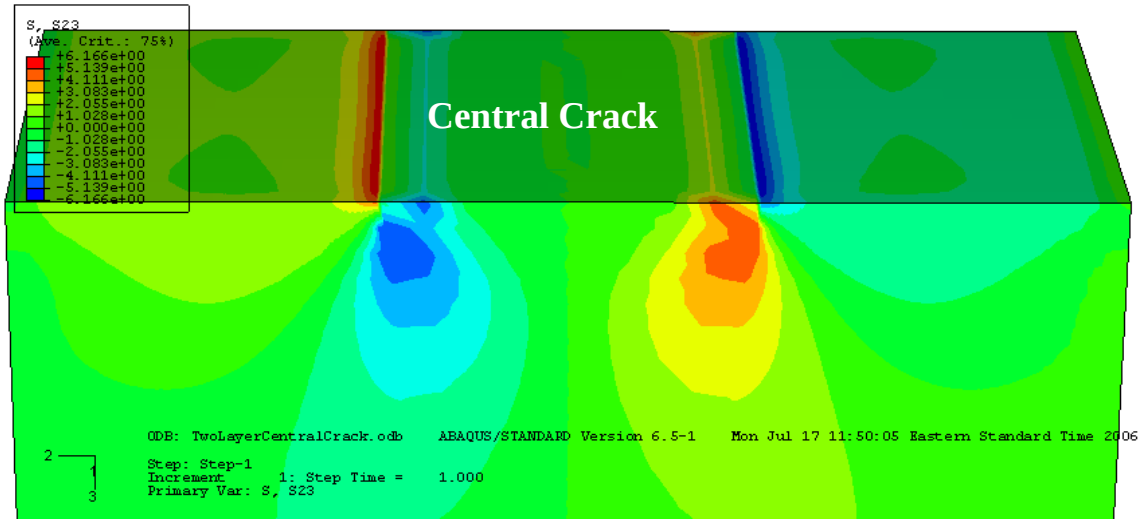

(Shear Stress Contours for Concrete Portion)

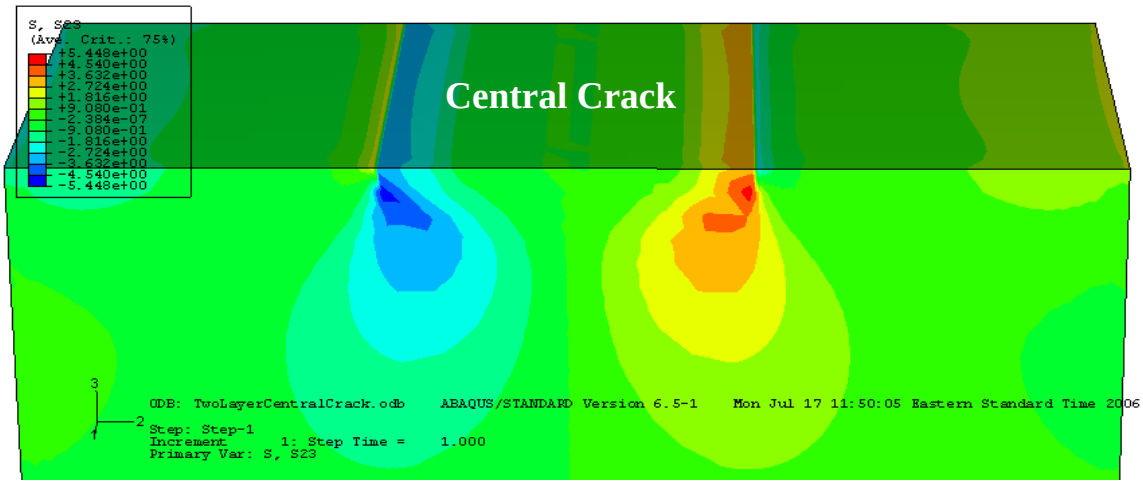

(Shear Stress Contours for Asphalt Portion)

Fig. 4.9 Shear Stress Contours for Central Crack Sample

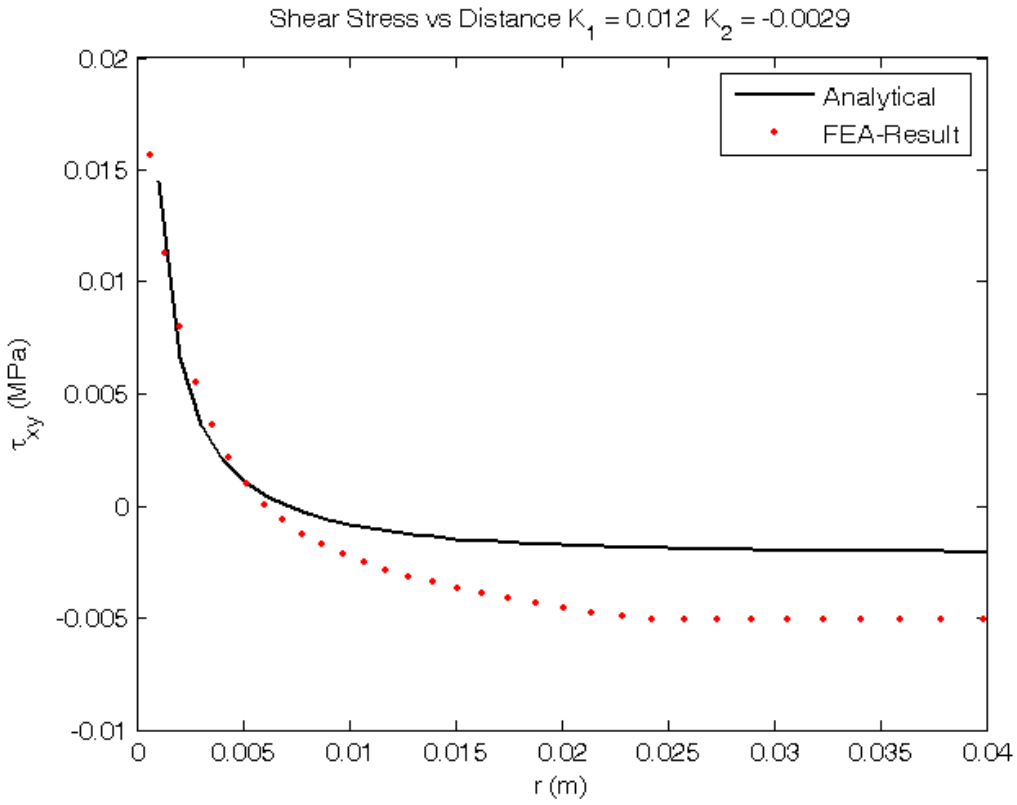

Fig. 4.10 Comparison of FEA and Analytical Shear Stress Distributions for Central Crack Sample

4.3 FEA Results for Edge Crack Geometry

FEA modeling was also conducted on composite block samples with a 2" edge interface crack geometry. The loading and boundary conditions for this model are identical to that previously described for the central crack case. The meshing process followed the same bias seeding technique producing the mesh shown in Fig. 4.11. The total number of elements in the edge crack model was 59,472 .

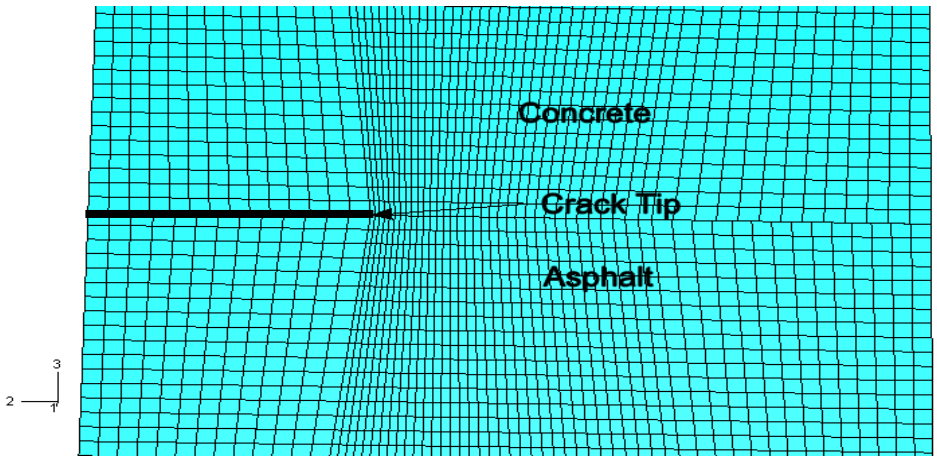

Fig. 4.11 Local View of the Mesh Near the Edge Crack

FEA stress results for this model are shown in Figs. 4.12 and 4.13. The normal stress S_{33} contours are shown in Fig. 4.12, and again we observe the high local stresses at the crack tip. Fig. 4.13 illustrates the shear stress S_{23} contours for the edge crack as shown in Fig 2.5.

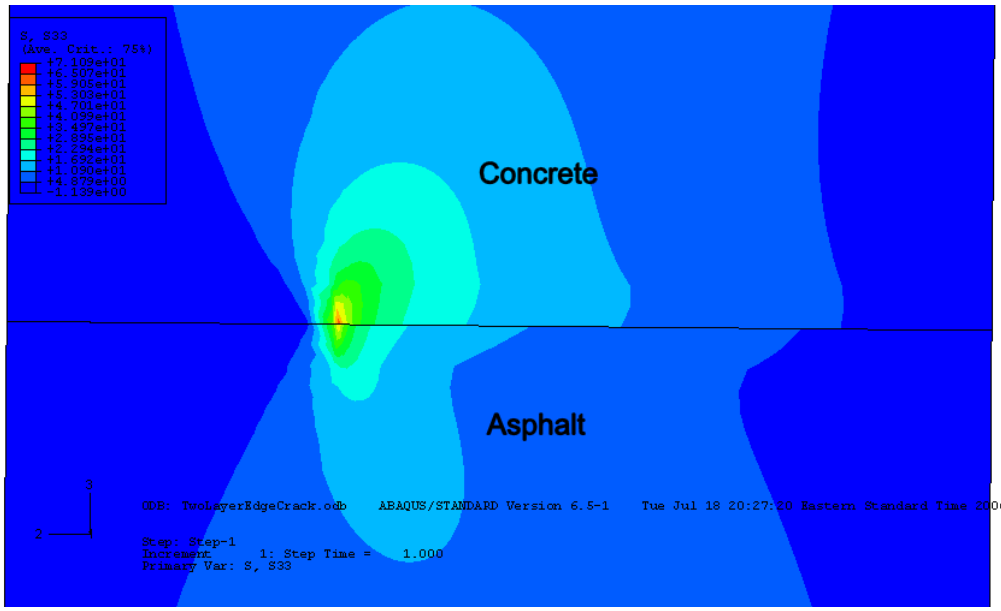

Fig. 4.12 Normal Stress Contours for Edge Crack Geometry

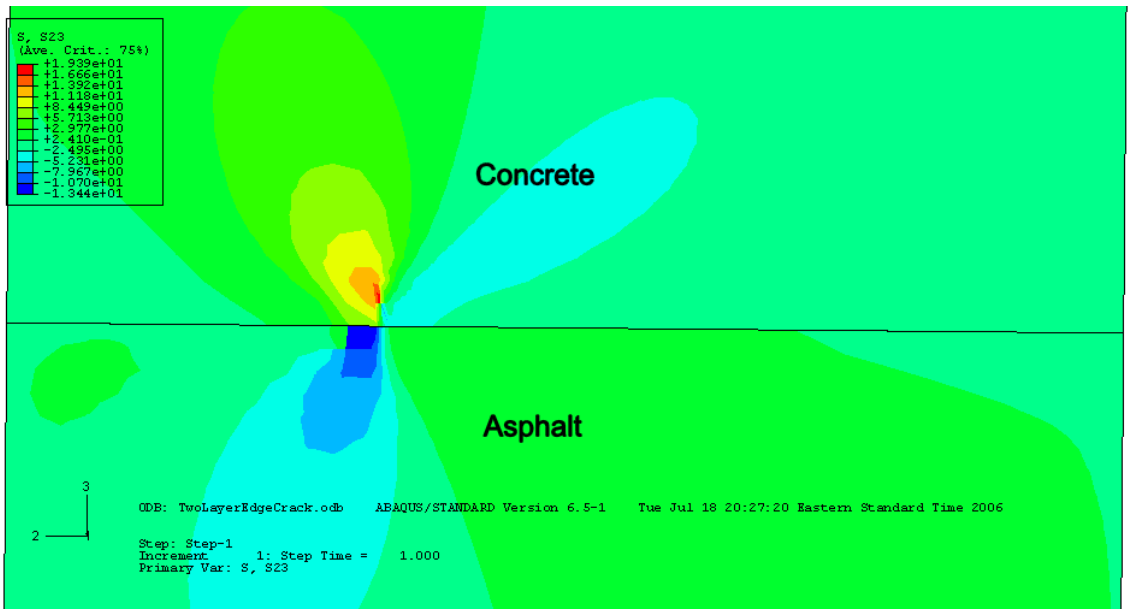

Fig. 4.13 Shear Stress Contours for Edge Crack Geometry

As with the central crack model, we wish to further explore the detailed FEA stress distributions along the interface in front of the crack. Fig. 4.14 illustrates the FEA normal stress results as a function of distance from the edge crack tip, and Fig. 4.15 shows the corresponding results for the shear stress component. Distribution results are qualitatively similar to the previous central crack results. Unfortunately, for this case no closed-form analytical solution exists, and thus no comparison can be made between FEA and theory.

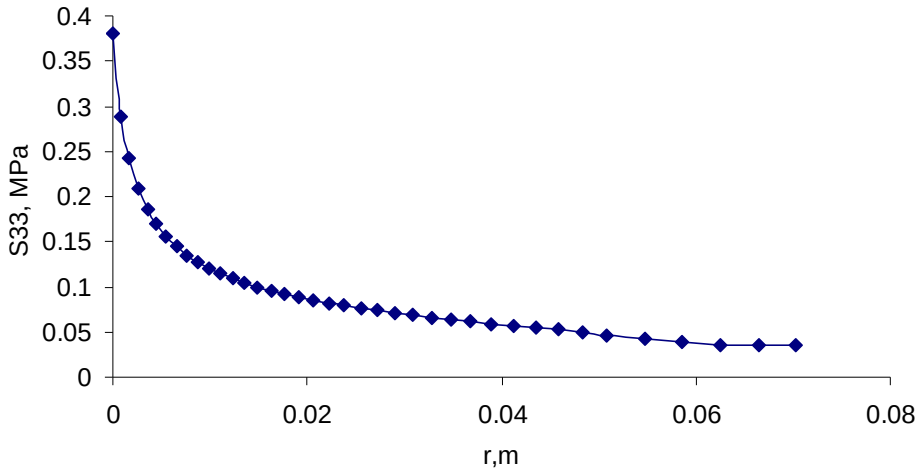

Fig. 4.14 Normal Stress Distribution for Edge Crack Model

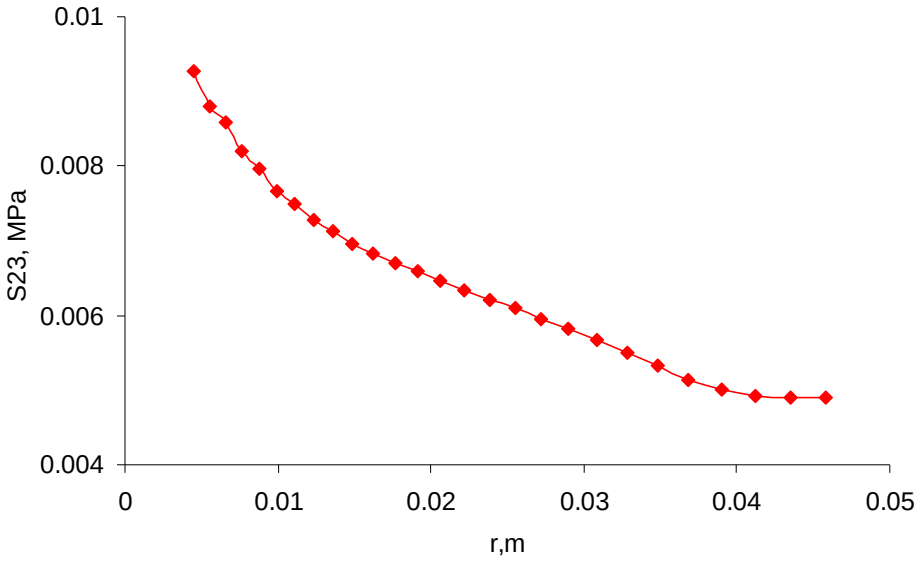

Fig. 4.15 Shear Stress Distribution for Edge Crack Model

CHAPTER V: STATIC AND DYNAMIC CHARACTERIZATION OF LAP JOINT SAMPLES

5.1 Introduction

It is well known that both concrete and asphalt exhibit rate dependent material behavior, and thus a composite concrete/asphalt system will likewise have deformation and failure behaviors that depend on loading or strain rate. Some traffic loadings from sudden starting and stopping or accident scenarios can produce high loading/strain rates that are no longer quasi-static. Thus some layered pavements can be subjected to such dynamic loadings and knowledge of rate dependent behavior would be useful to understand the roadway response . We now wish to explore the effect of loading rate on laboratory composite lap joint samples, and compare static failure behaviors with those found under dynamic loading.

High strain rate laboratory test data may be generated using a variety of methods depending on the test-piece size and the energy or velocity demands of the experiment. For example, *Charpy* impact pendulum machines employ an instrumented hammer that is swung into a notched square or rectangular specimen bridged across a set of anvils that are positioned in the hammer's path. This gives rise to specimen strain rates in the order of $10\text{-}10^2$ in/in/s with resultant impact energies of up to 600 joules. *Drop weight* impact testing machines employ a guided free falling or spring-assisted weight and puncture probe. These machines develop similar strain rates but are capable of generating impact energies of 60,000 joules. Higher strain rates can be achieved using *Hopkinson Bars* and *Gas Guns* that rely on force transmission by a gas pressure assisted rod or by actual projectile firing. These devices lead to strain rates typically from $10^2\text{-}10^3$ in/in/s, and energies up to 600,000 joules. With the availability of a Hopkinson Bar in our laboratory, we decided to use this device for our dynamic testing.

In order to study dynamic behavior, modification to our original specimen geometry was required. With the desire to apply dynamic loadings using a Hopkinson Pressure Bar apparatus, it was decided to limit our investigation to lap joint samples tested under shear loading. The lap joint sample geometry for these studies is shown in Fig. 5.1 and consisted of a composite asphalt-concrete specimen of cylindrical shape with an interface lying along the cylinder's axis. The sample is to be loaded with compressive end forces and the location of the interface along the loading direction will eliminate bending effects and thereby subject the interface to primarily

shear loading. Because of the limited interface area, no interface crack was introduced in this sample. Details on the sample preparation were previously given in Section 2.8.

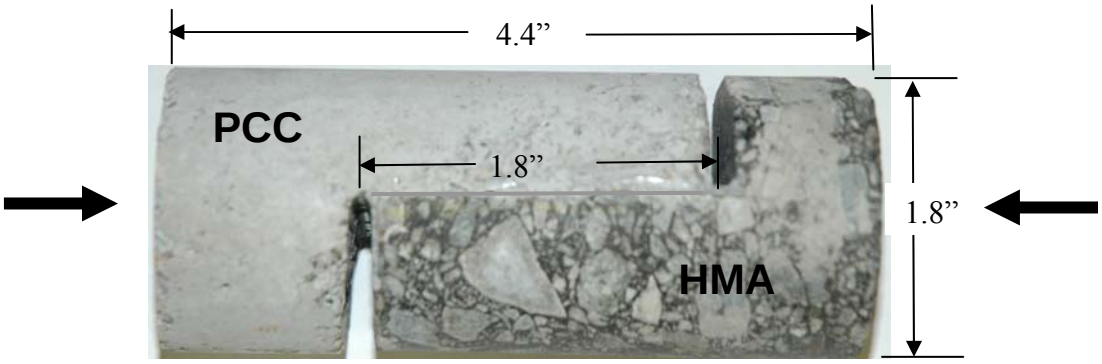

Fig. 5.1. Lap Joint Specimen Geometry

5.2 Static Lap Joint Testing

In order to compare with our planned dynamic test results, a series of static lap joint tests were conducted. Static compression tests on these composite samples were conducted on an Instron testing machine (see Fig. 5.2) to determine the shear strength. Shear strength was determined by simply dividing the failure load by the bonded interface area. A typical load extension curve is illustrated in Fig. 5.3 showing the rapid load loss at failure. Peak loads were used to determine the average failure shear stress.

Fig. 5.2 Lap Joint Sample Under Quasi-static Loading

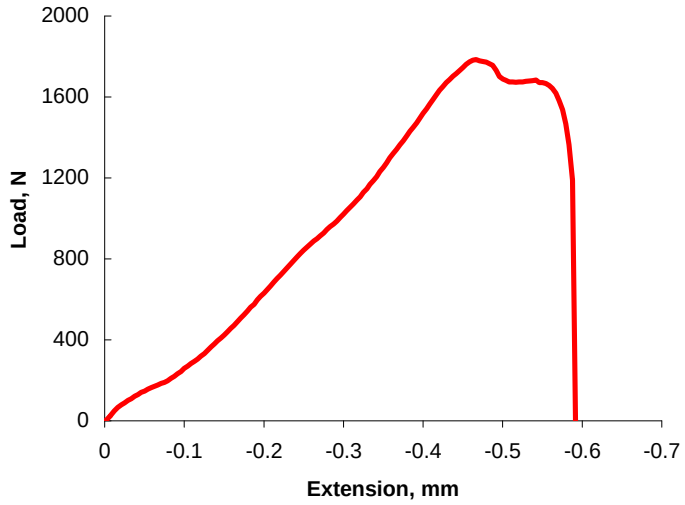

Fig. 5.3 Load Extension Behavior of Lap Joint Sample

A postmortem photograph of a failed sample under static loading is illustrated in the Fig 5.4. As shown some particular asphalt pullouts are evident on the concrete side of the failed interface thus indicating some inelastic interfacial failure.

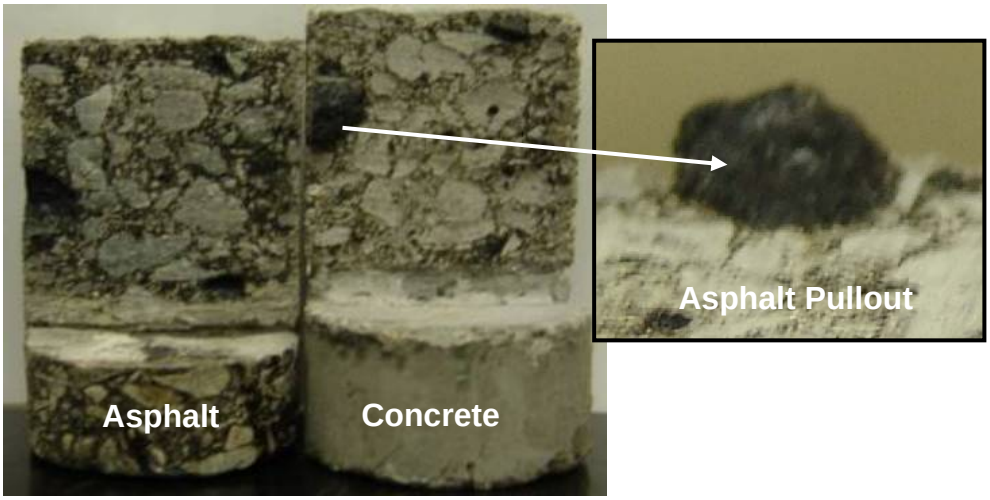

Fig. 5.4 Postmortem Photograph of Failed Lap Joint Sample. Enlarged Surface View Shows Asphalt Pullouts on Concrete Surface

A set of seven static compression tests were conducted, and the results are summarized in Table 3. The average static interface shear strength was found to be 0.75MPa, and this value will be compared with the corresponding dynamic results.

Table 5.1 Static Lap Joint Compression Test Results

Sample No.	Area, mm^2	Failure Load		Static Shear Strength	
		kN	lbs	MPa	psi
1	1975	1.49	335.70	0.76	109.72
2	2088	1.78	400.50	0.85	123.60
3	2032	1.62	364.50	0.80	115.61
4	2079	1.55	348.75	0.76	110.74
5	2032	1.25	281.25	0.62	89.22
6	2032	1.59	357.75	0.78	113.49
7	2032	1.39	312.75	0.68	99.21
Average Static Shear Strength				0.75	108.80
Standard Deviation				0.08	11.31
95% Confidence				0.057	8.4

5.3 Split Hopkinson Pressure Bar Apparatus

The dynamic loading device used is known as a *Spilt Hopkinson Pressure Bar* (SHPB), named after its original developers John and Bertram Hopkinson; although H. Kolsky is credited with the split-bar arrangement used in most current day set ups. The use and applicability of SHPB testing to determine dynamic behaviors of a very wide variety of materials (metals, polymers, ceramics, rock, concretes, etc.) is well documented in the literature.

The conventional SHPB apparatus consists of a striker bar, an incident bar and a transmitter bar, as illustrated in Fig 5.5. The specimen under study is placed between the incident and transmitter bar. A projectile fired from a gas gun impacts the incident bar. This impact generates a compressive stress pulse of a finite length in the incident bar, which travels towards the specimen. The amplitude of the stress pulse is a function of the velocity of the striker bar, and its period is approximately equal to twice the wave travel time in the striker bar. Upon reaching the incident bar-specimen interface, the incident wave gets partly reflected back and partly transmitted into the specimen depending on the impedance and area mismatch between the specimen and bar. Previous analyses have established that the transmitted pulse amplitude is a measure of stress in the specimen while the amplitude of the reflected pulse is a measure of specimen strain rate. Thus upon integrating the reflected pulse, the strain in the specimen can be determined. The specimen can be subjected to a wide range of strain rates by employing striker bars of various lengths. As suggested by Tekalur et al. (2004) for bituminous material testing, the conventional transmitted bar of hardened steel was replaced by the hollow aluminum bar to avoid large impedance mismatch. An 3.15" long striker bar projectile was used in the study, and a thin layer of lubricant was applied on each sample end to minimize the friction effects.

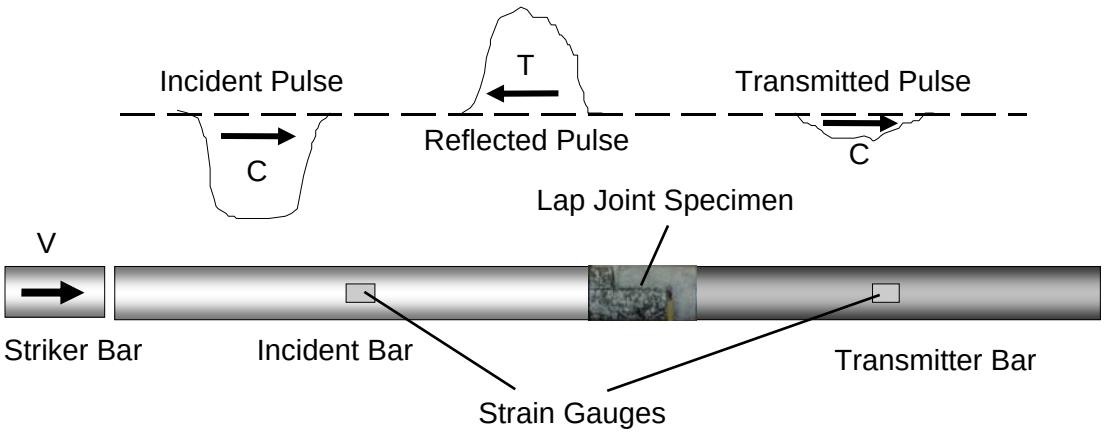

Fig. 5.5 Schematic of Split Hopkinson Pressure Bar Apparatus

The fundamental relations used to analyze and characterize the dynamic loading system is based on the classical D'Alembert, one-dimensional wave equation solution given by

$$u(x,t) = f(x - c_o t) + g(x + c_o t) \tag{5.1}$$

where *f* corresponds to a wave traveling in the positive *x*-direction (to the right), *g* corresponds to a wave traveling in the negative *x*-direction, and $c_o = \sqrt{E/\rho}$ is the wave speed in the bar material with modulus *E* and density ρ. From one dimensional rod theory, the displacements at the left and right specimen-bar interfaces can be expressed in terms of the incident, reflected and transmitted strains

$$\begin{aligned} u_1 &= c_o \int_0^t (-\varepsilon_i + \varepsilon_r) dt \\ u_2 &= -c_o \int_0^t \varepsilon_t dt \end{aligned} \tag{5.2}$$

The average strain the specimen, ε_s, is then given by,

$$\varepsilon_s = \frac{c_o}{l_s} \int_0^t (\varepsilon_i - \varepsilon_r - \varepsilon_t) dt \tag{5.3}$$

where l_s is the original length of the specimen. The loads at the left and right specimen/bar interfaces can be expressed by

$$\begin{aligned} P_1(t) &= A_b E_b [\varepsilon_i(t) + \varepsilon_r(t)] \\ P_2(t) &= A_b E_b \varepsilon_t(t) \end{aligned} \tag{5.4}$$

where E_b and A_b are the modulus and cross-sectional area of the bars. Now it is normally assumed that the loading pulse wavelength is larger than the sample length and thus wave propagation effects within the specimen may be neglected. Under these conditions, we have the usual equilibrium condition such that $P_1 = P_2$, and thus it follows that $\varepsilon_i + \varepsilon_r = \varepsilon_t$. Using these results, relation (5.3) then gives

$$\varepsilon_s(t) = \frac{-2c_o}{l_s}\int_0^t \varepsilon_r dt \tag{5.5}$$

and the average stress in the specimen is then given by,

$$\sigma_s = E_b \frac{A_b}{A_s}\varepsilon_t \tag{5.6}$$

where A_s is the cross-sectional area of the sample.

The previous derivations are based on one-dimensional wave theory that assumes there is no variation in stress or strain over the cross-sections of the bar or sample, thereby allowing measured surface strains to represent the internal strains. It has been observed that the major portion of the generated wave motion is contained in wavelengths that exceed 10*R*, where *R* is the radius of the bars. Under such conditions, wave theory indicates that a one-dimensional deformation assumption is reasonable. Also under this type of wave motion, the stress pulses should suffer minimal dispersion.

5.4 SHPB Test Results

Fig. 5.6 illustrates a close-in photograph of the sample in the SHPB loading apparatus. Specimen ends were carefully manufactured to ensured flat and smooth contact with the neighboring bar, and a thin layer of lubricant was used at each end to minimize friction effects. A series of five dynamic tests were performed on composite lap joint samples using this scheme.

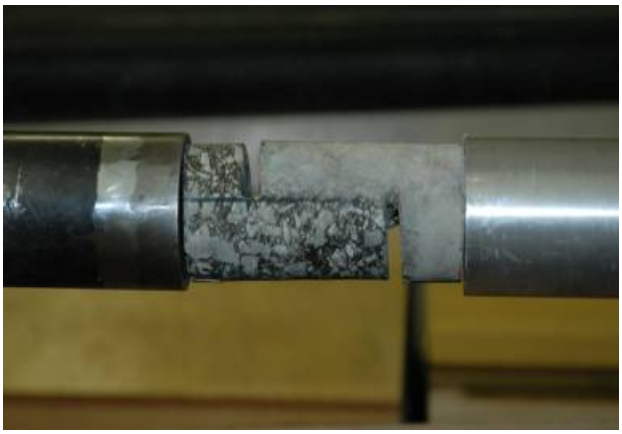

Fig. 5.6 Dynamic Lap Joint Testing Setup

A typical load time history obtained from the SHPB testing is shown Fig 5.7, and this gave a loading rate of about 300N/μsec. Again the peak value of this profile was used as the failure load, and it was verified that the sample was in approximate equilibrium during this time period. Fig. 5.8 shows a postmortem photograph of a failure sample from the dynamic testing. Contrary to the previous static results, the lap joint now failed in a clean interfacial mode with no observed asphalt pullout at the interface.

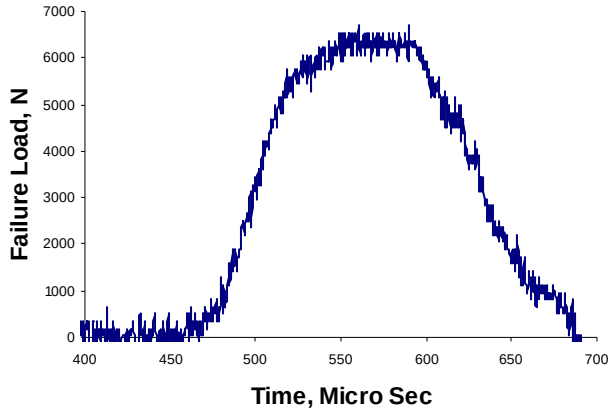

Fig. 5.7. Typical Load Time Profile From Dynamic Test

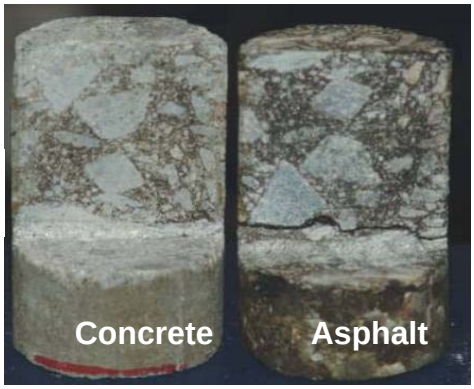

Fig. 5.8 Postmortem Photograph of Failed Lap Joint Sample Under Dynamic Loading

Dynamic test results for a series of five SHPB experiments are shown in Table 5.2. Recorded failure load values showed some variation which is expected for such cementous materials with random particulate reinforcement. The average dynamic shear strength was found to be as 2.9MPa, which was 4 times the static shear strength given in Table 5.1. Such increases in dynamic strength have been found for other materials.

Table 5.2 Dynamic Compression Test Results

Sample No.	**Area, mm^2**	**Failure Load**		**Dynamic Shear Strength**	
		kN	**klb**	**MPa**	**kpsi**
1	1976	5.4	1.22	2.75	0.40
2	1987	5.9	1.33	2.97	0.43
3	2032	6.2	1.40	3.06	0.44
4	2134	6.7	1.50	3.13	0.45
5	2032	5.3	1.20	2.62	0.38
Average Dynamic Shear Strength				2.91	0.42
Standard Deviation				0.21	0.03
95% Confidence				0.19	0.03

CHAPTER VI – COMPOSITE INDIRECT TENSION TESTING

6.1 Introduction

Because of the difficulty in achieving true interfacial failure in the direct tension tests on the composite rectangular block samples shown previously in Fig. 2.1, it was decided to explore the possibility of using a composite indirect tension geometry. This concept was first suggested by Soares and Tang (1998) and was referred to as a *Bimaterial Brazilian Specimen.* Fig 6.1 illustrates the basic idea where a standard IDT sample would be composed of half asphalt and half concrete with an interface. Orienting the specimen such that the applied compression loading acts along the interface would tend to create a tensile stress field in the direction perpendicular to the interface. This situation will offer the prospect of using the standard ASTM cylindrical samples (or core samples) that could be conveniently cut and fabricated into specimens for interface debonding studies. Based on these prospects, a few such samples were fabricated and tested. Preliminary finite element analysis was conducted on this geometry in order to explore the nature of the stress field along the interface.

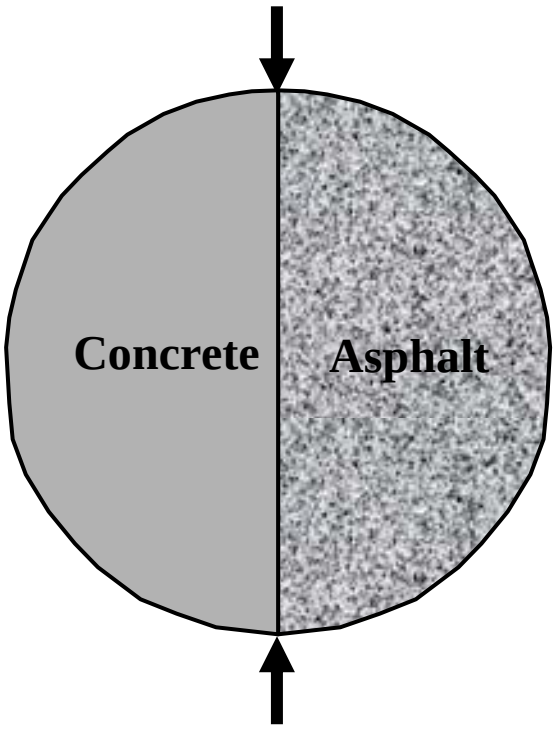

Fig. 6.1. Composite IDT Sample

6.2 Composite IDT Sample Preparation

The sample preparation for this specimen is illustrated in the sequence of operations in Fig. 6.2. The process started with a roadway core sample provided by RIDOT as shown in Fig. 6.2(a). This was cut to dimensions of the standard ASTM IDT sample size of 4" (101.6mm) diameter and 2.5" (63.5mm) thickness as shown in Fig. 6.2(b). This portion of material was assumed to be the top course, Class I-1 pavement. This sample was then cut along the diameter and was placed in the plastic mold as shown in the Fig.6.2(c). Fig.6.2(d) shows the concrete that was poured in to the mold to complete the composite sample. The final result is shown in Fig. 6.3.

Fig. 6.2 (a) Core Sample from Roadway

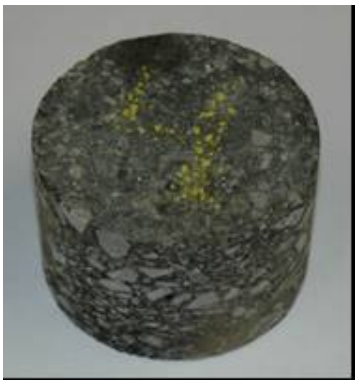

Fig. 6.2 (b) Class I-1 Sectioned Sample

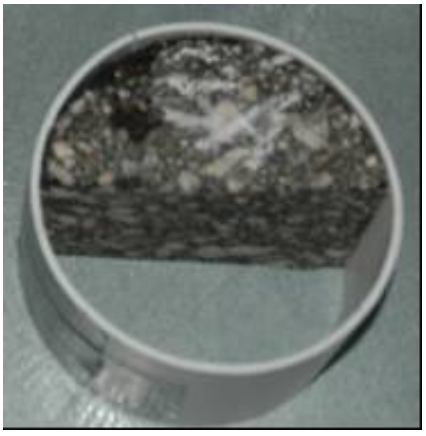

Fig. 6.2 (c) Cut Sample in the Mold

Fig. 6.2 (d) Concrete Filled Half

Fig. 6.2. Sequence of Operations for Compoiste IDT Sample Preparation

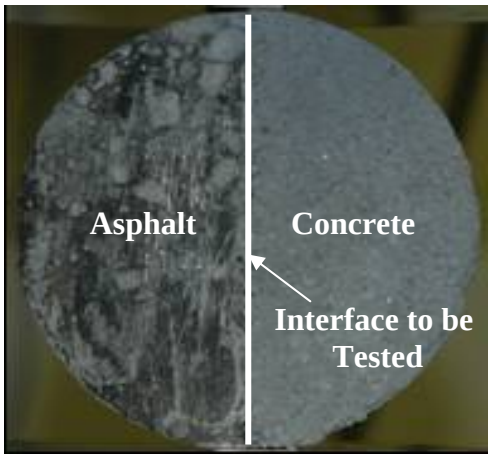

Fig. 6.3 Completed Composite IDT Sample

6.3 Testing and Results

As shown in Fig. 6.4, composite IDT samples were tested in two different orientations: one with the interface parallel to loading and the other perpendicular to the loading axis. In this fashion we could explore the effects of tensile stress fields both normal and tangential to the concrete/asphalt interface.

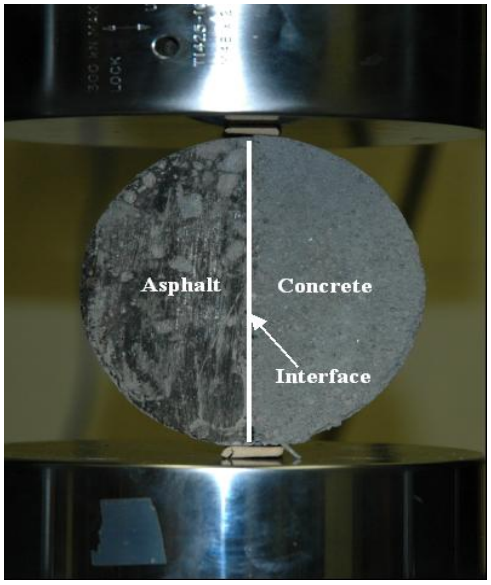

(a) Interface Parallel to Loading

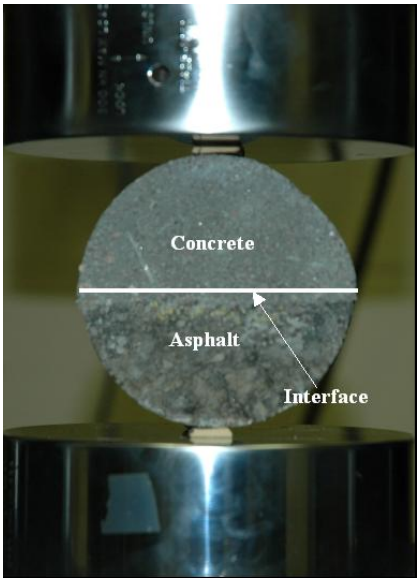

(b) Interface Perpendicular to Loading

Fig. 6.4 Two Different Loading Orientations for IDT Testing

Testing involved three samples at each orientation along with two homogeneous asphalt samples. The loading rate was maintained at 2.5mm/min for all tests. Results are summarized in Table 6.1. The test results indicate that the load at failure for the interface parallel to loading was lower than for the case with interface perpendicular to loading. A typical load-extension curve for each test is shown in Fig 6.5. It is observed that the failure load occurs at approximately the same extension value. Fig. 6.6 illustrates a typical post mortem picture of the IDT sample with orientation interface parallel to the loading direction. Failure of this type of sample was primarily interfacial with very little asphalt pullouts. This is in striking contrast to the observed failures found in the rectangular block samples as shown in Fig 3.9. The failure for the sample tested with interface perpendicular to loading showed no failure in the interface but there was transverse cracking found in the area of loading as shown in Fig. 6.7.

Table 6.1 Composite IDT Test Results

Sample No.	**Failure Load, kN**
Interface Parallel to Loading	
1	8.4
2	9.2
3	9.1
Interface Perpendicular to Loading	
1	12.4
2	12.5
3	18.3
Homogeneous Asphalt Material	
1	6.7
2	6.1

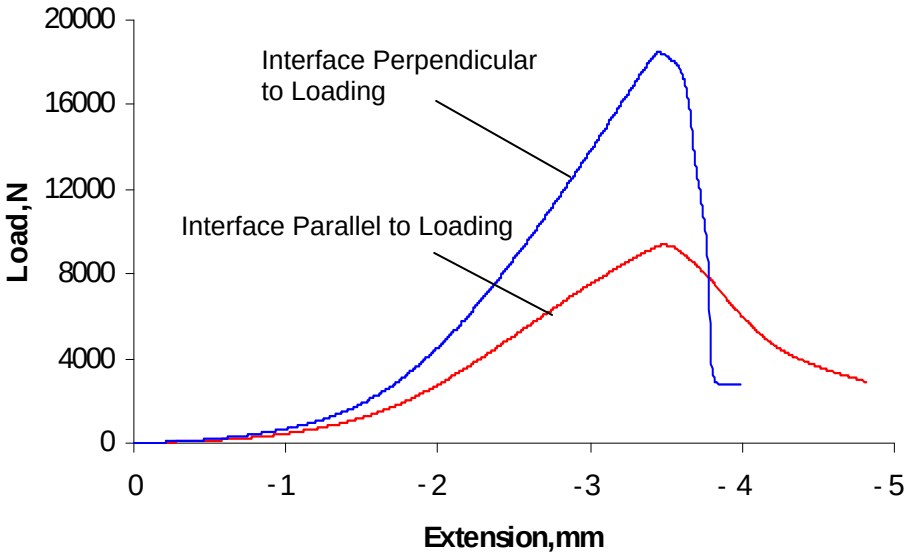

Fig. 6.5. Load Extension Curves for Composite IDT Samples with Different Interface Orientations

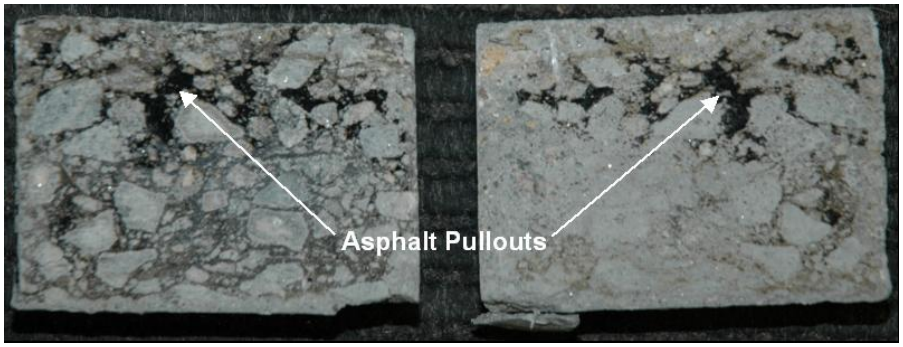

Fig. 6.6. Postmortem Failure of Sample Tested with Interface Parallel to the Loading

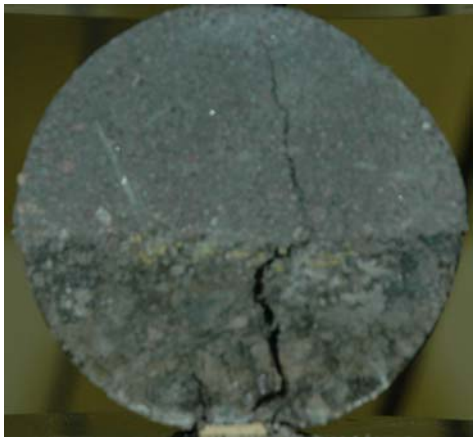

Fig. 6.7. Postmortem Failure of Sample with Interface Perpendicular to the Loading

6.4 Finite Element Simulation

The standard elasticity relation (2-2) cannot be used to determine the splitting stress of this non-homogeneous sample, and thus finite element simulation must be employed to conduct the bimaterial stress analysis. FEA simulations were run for both homogeneous asphalt and the composite bimaterial sample. A pressure loading of 500lb resultant was applied at the sample's top and the bottom was fixed over the bearing area.

For the homogeneous sample, contours of the horizontal normal stress S_{11} are shown in Fig. 6.8. As expected for the homogeneous case, the stress field distribution indicates a constant stress region along the direction of loading. The value of this stress component is plotted versus distance from the bottom of the sample in Fig. 6.9. The simple elasticity prediction $\sigma = {}^{2P}\!/_{\pi DT}$ is also shown in the figure, and it is apparent that the FEA stress results match reasonably well with the analytical solution in regions away from the loading points. This gave us confidence that the FEA modeling was appropriate and could be used to explore the composite bimaterial sample.

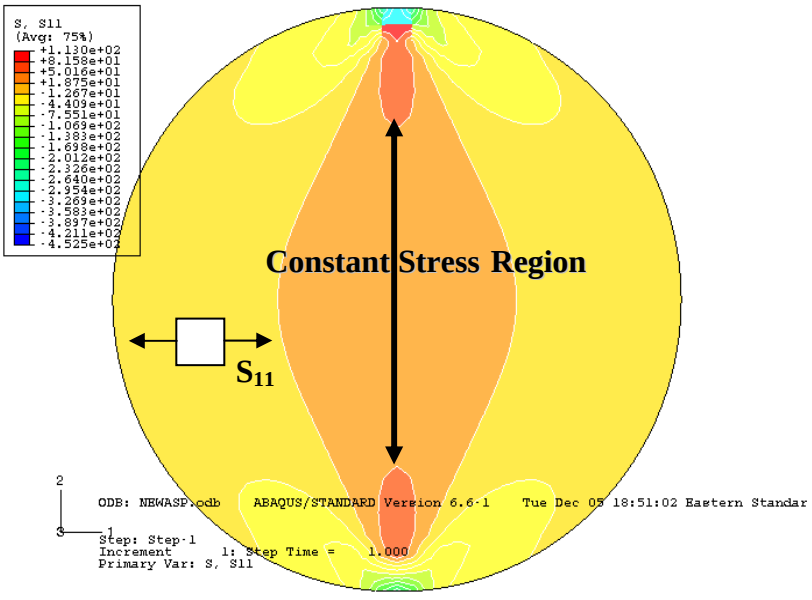

Fig. 6.8. S_{11} Tensile Stress Contours for a Homogeneous Asphalt Material

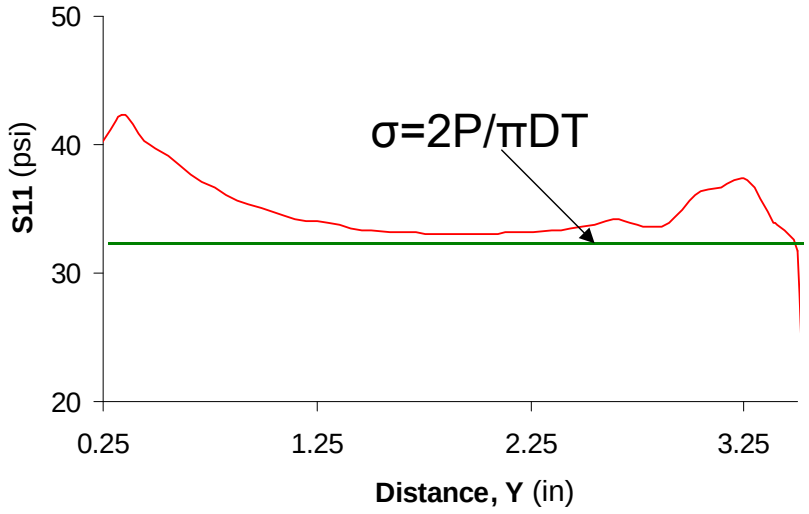

Fig. 6.9. S_{11} Tensile Stress Distribution for Homogeneous Sample

FEA modeling for the composite IDT sample was developed with a perfectly bonded interface thus implying infinite bond strength. Fig. 6.10 illustrates contours of the horizontal normal stress S_{11}, and it is noted that the contours are no longer symmetric with respect to the vertical. However, the FEA results indicate that there is also an approximate constant stress zone along the interface, and this fact confirms that such IDT tests could be used to determine the interfacial strength of the sample. The distribution of the interfacial S_{11} stress versus distance from the bottom of the sample is shown in Fig. 6.11. These stress values were taken as the average value from each material side. For this non-homogeneous case, the elasticity prediction $\sigma = {}^{2P}\!/_{\pi DT}$ will not hold but the FEA result can be used instead by say using the average value given by the dotted line in Fig. 6.11. Although this FEA simulation was for a single loading case, further simulations can be run to determine the splitting stress as a function of the applied loading. Thus a series of FEA simulations could replace the simple elasticity stress relation. In conclusion, the stress at the interface of these FEA models can be compared with the corresponding results for the rectangular model to perhaps gain a better understanding of the interfacial failure. Further research is needed to determine if these preliminary findings would indeed lead to a better sample geometry for interfacial failure studies.

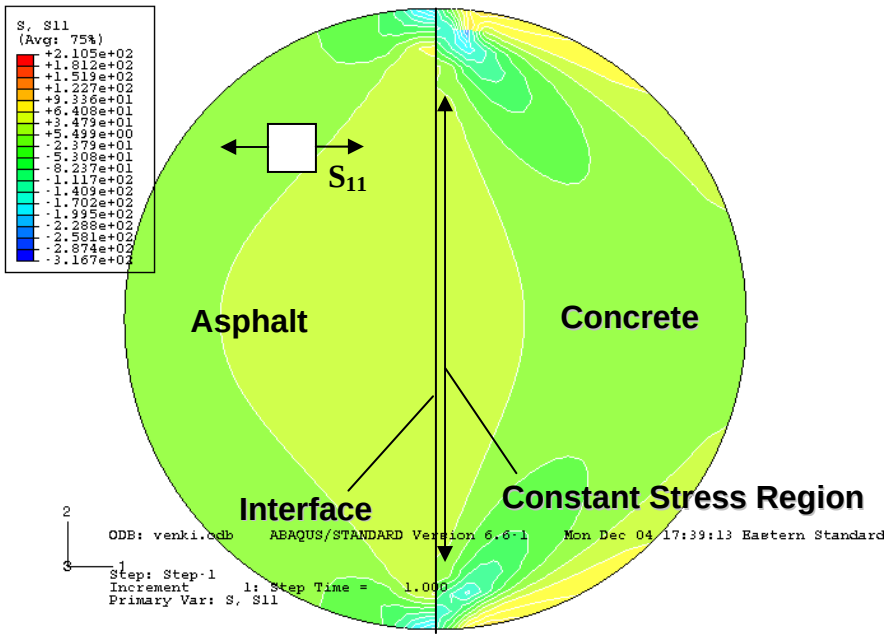

Fig.6.10. S_{11} Tensile Stress Contours for Composite Sample

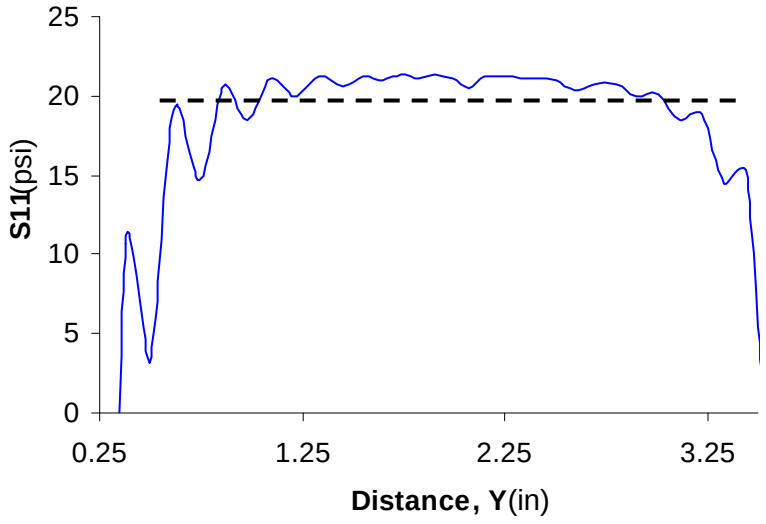

Fig. 6.11. S_{11} Tensile Stress Distribution for Composite Sample

CHAPTER VII – SUMMARY, CONCLUSIONS AND RECOMMENDATIONS

7.1 Summary and Conclusions

The presented work has experimentally investigated static and dynamic interfacial failure between concrete and asphalt materials related to roadway applications. Static studies were conducted on composite samples with central interface crack geometry. Specimens were created using laboratory material of two different age groups: 30 and 200 day-old and some samples were created from cores taken from a local Rhode Island whitetopping site. For the laboratory samples, it was found that the older material had average interface strength about twice as large as the newer material. Likewise, critical stress intensity factors (fracture toughness) for samples with older asphalt were also about twice that of the samples with 30 day-old asphalt. For the core sample specimens, it was found that the failure loads and resulting critical stress intensity factors were higher than those observed in the laboratory samples. Since the core samples were likely several years old, this behavior follows the aging effects found in the laboratory sample data set. It was also observed for the core sample tests that the interfacial failure was more brittle-elastic with relatively little inelastic deformation along the concrete-asphalt surface.

Tests were also conducted on laboratory samples with an interface inclined to the loading direction, and these results showed an increase in fracture toughness by a factor of 2 when compared to the aged non-inclined interface crack specimens. Similar to results of previous studies on other bi-material systems, the interface fracture toughness was found to be less than that of either homogenous concrete or asphalt. This finding would suggest that fracture should occur along the interface; however, it was observed that sample failure generally occurred in the asphalt material near the interface. This behavior would indicate that other mechanisms are at work and it is felt that perhaps the micromechanical nature of each material contributes to this failure response. Specifically the particulate reinforced nature of asphalt can produce high inter-granular stresses thereby biasing crack growth into the binder component.

Because of the problem in achieving true interfacial fracture behavior in the laboratory block specimens, we also explored the use of a composite indirect tension sample made of two semi-circular half-portions of concrete and asphalt. This represented a new sample geometry, and preliminary finite element analysis showed that a reasonably uniform tensile stress field would act normal to the concrete/asphalt interface. Some beginning laboratory test results

indicated that sample failure was indeed interfacial with a relatively clean fracture along the concrete/asphalt interface.

Dynamic studies employed a different sample geometry using a composite lap joint specimen. Because of the small specimen size, lap joint samples had no initial interface crack and thus the collected data could only be used to determine average shear strength of the asphalt-concrete interface. The lap joint was tested in both quasi-static loading using an Instron machine and dynamic loading using a Spilt Hopkinson Pressure Bar (SHPB) apparatus. Although each type of loading produced interfacial shear failure, static tests showed some asphalt pullout while the dynamic samples showed smooth failure surfaces with no observed pullouts of either material. Dynamic shear strength of the composite lap joint samples was found to be about four times the static strength.

7.2 Recommendations

Based on the results of this study, it is suggested that further investigations be made in the following areas:

- Conduct more sample testing on actual roadway material taken from different sites with different construction and traffic loading history.
- Implement the use of strain gauges near the interfacial crack tip to evaluate fracture mechanics parameters. Initial work attempted this but time limitations did not allow us to complete the task.
- Conduct more laboratory testing on samples with inclined interfaces at several different angles to explore the mixed mode effect in more detail. Also conduct finite element analysis on such samples.
- Investigate lap joint samples with initial interface cracks. This may require the use of slightly large specimens.
- Conduct quasi-static testing of composite IDT samples with existing interfacial cracks.
- Conduct high strain rate loading using SHPB on composite IDT samples and include cases both with and without existing interfacial cracks.
- Further explore the use of cohesive zone modeling of the interfacial failure behaviors.

REFERENCES

Chen, D. and Cheng S., March 1983, “An analysis of adhesive-bonded single lap joints.” Journal of Applied Mechanics, Vol. 50, pp.109-115

Cho, Y. H. and Koo, H. M. (2003), “A Behavior Analysis of Concrete Overlay Based on the Characteristics of Asphalt Pavements”, Proceedings of 82nd Transportation Research Board Meeting, Washington, D. C.

Comninou, M., 1990, “An Overview of Interface Cracks.” Engineering Fracture Mechanics, Vol. 37, 197-208.

Hutchinson, J. W., Mear, M. E. and Rice, J. R. (1987), “Crack paralleling an Interface Between Dissimilar Materials”, Journal of Applied Mechanics, Vol.54, pp. 828-832.

Kumara, W., Tia, M., Wu,C-L, and Choubane, B., (2003), “Evaluation Of Applicability Of Ultra Thin Whitetopping In Florida”, Transportation Research Record, No:1823.

McBride, S., Shukla, A. and Bose, A., (2002), “Processing and Characterization of a Lightweight Concrete Using Cenospheres”, Jour. of Materials Sci., Vol 37, pp 4217-4225.

Nelson, P. K. and Rasmussen, R. O. (2002), “Delamination Stresses at the Interface of Bonded Concrete Overlays”, Proceedings of 81st Transportation Research Board Meeting, Washington, D. C.

Nishiyama, T., Bhatti, M. A. and Lee, H. D. (2003), “Development of 3D Finite Element Model to Quantify Bond Level of Thin Concrete Overlay”, Proceedings of 82nd Transportation Research Board Meeting, Washington, D. C.

Ricci, V., Shukla, A., and Singh, R. (1997), “Evaluation of Fracture Mechanics Parameters in Bimaterial Systems Using Strain Gages”, Engineering Fracture Mechanics, Vol. 58, No. 4, pp. 273-283.

Rice, J. R. (1988), “Elastic Fracture Mechanics Concepts for Interfacial Cracks”, Jour. of Applied Mechanics, Vol. 55, pp. 98-103.

Rice, J.R., Sih, G.C., 1965, “Plane Problems of Cracks in Dissimilar Media.” Journal of Applied Mechanics, Vol. 32, 418-423.

Rice, **J.** R., Suo, Z. and Wang, J.-S., (1990), "Mechanics and thermodynamics of brittle interfacial failure in bimaterial systems," Metal-Ceramic Interfaces, Acta-Scripta Metallurgica, Series 4, pp. 269-294.

Rossamanith, H.P. and Shukla, A., “Dynamic Fracture of Imperfectly Bonded Lap Joints”, ingenieur-Archive, Vol.51 1981,pp.275-285.

Sadd, M.H., (2005), Elasticity: Theory, Applications and Numerics, Elsevier Science, Burlington, MA.

Shah. S., Swartz. S., and Ouyang. C., "Fracture Mechanics in Concrete", John Wiley Sons, Inc., New York, 1995 pp.134.

Shukla, A., Srivastava, V., and Parameswaran, V. (2000), "Experimental Evaluation of the Dynamic Shear Strength of Adhesive Bonded Lap Joints", Jour. of Testing and Evaluation, Vol. 28, pp 438-442.

Soares, J.B. and Tang, T., (1998), "Bimaterial Brazilian Specimen for Determining Interfacial Fracture Toughness", Eng. Frac. Mech., Vol. 59, pp 57-71.

Tekalur,A,S "Characterization of Recycled Asphalt Pavement Concrete under Static and Dynamic Loads", MS Dissertation (2004), University of Rhode Island, USA.

Vandenbossche, J. M. and Fagerness, A. J. (2002), "Performance and Repair of Ultra-Thin Whitetopping: The Minnesota Experience", Proceedings of 81st Transportation Research Board Meeting, Washington, D. C.

Williams, M.L., 1957, "On the Stress Distribution at the Base of a Stationary Crack." Journal of Applied Mechanics, Vol. 24, 109-114.

Williams, M.L., 1959, "The Stresses Around a Fault or Crack in Dissimilar Media." Bulletin of the Seismological Society of America, Vol. 49, 199-204

Zachary,L.W. and Burger, C.P., May 1980, "Dynamic wave propagation in a single lapjoint." Ingenieur-Archive 51, pp. 275-285

PRESENTATIONS OF WORK

During the duration of this research program, several presentations of the work were given at various meetings and conferences as listed below:

- 18th Annual Rhode Island Transportation Forum, University of Rhode Island, November 4, 2005.
- TRB Pavement Performance & Data Analysis Forum, Washington, D.C., January, 21, 2006
- Annual TRB Visitation Meeting, University of Rhode Island, May, 24, 2006
- 2006 Annual Meeting of Society of Experimental Mechanics, St Louis, MO, June 5, 2006
- 19th Annual Rhode Island Transportation Forum, University of Rhode Island, November 3, 2006.
- 2007 Annual Meeting of Society of Experimental Mechanics, Springfield, MA, June 3-6, 2007
- 20th Annual Rhode Island Transportation Forum, University of Rhode Island, November 2, 2007.